Coordinated Hybrid Control of Satellite Formations

Tord H. Aune

June 5, 2006

Departement of Engineering Cybernetics
Norwegian University of Science and Technology
Trondheim Norway

NTNU
Norges teknisk-naturvitenskapelige universitet

Fakultet for informasjonsteknologi, matematikk og elektroteknikk
Institutt for teknisk kybernetikk

MASTEROPPGAVE

Kandidatens navn: Tord H. Aune

Fag: Teknisk Kybernetikk

Oppgavens tittel (norsk): *Koordinert hybrid regulering av formasjoner av satellitter.*

Oppgavens tittel (engelsk): *Coordinated Hybrid Control of Satellite Formations*

Oppgavens tekst:
The assignment relates to the spacecraft formation flying problem and the use of methods from the field of hybrid systems.

Oppgaver:

1. Present both a linear and nonlinear model for the position dynamics of a spacecraft formation.
2. Present relevant disturbances (J2) that need to be taken into account in the dynamics model.
3. Present the relevant theory and definitions of *Hybrid systems*,
4. Investigate how the use of thrusters as actuators fits into the framework of hybrid systems.
5. Investigate how the satellite formation flying problem fits into the framework of hybrid systems. Pay special attention to the problem of switching between different modes of operation.
6. Perform simulations of hybrid control of satellite formations using appropriate simulation tools.

Oppgaven gitt: 22/2-06

Besvarelsen leveres: 6/6-06

Besvarelsen levert:

Utført ved Institutt for teknisk kybernetikk

Veiledere: Esten I. Grøtli, NTNU

Trondheim, den

Jan Tommy Gravdahl
Faglærer

Preface

This thesis is a part of the requirements for the degree of Master of Science (Siv.ing) in Engineering Cybernetics, and has been carried out at the Norwegian University of Science and Technology, NTNU.

I would like to thank my supervisor Associate Professor Tommy Gravdahl for his valuable input and guidance throughout this semester. I would also like to thank my advisor Phd-student Esten I. Grøtli for his help and patience during the course of this thesis.

Tord H. Aune
Trondheim June 5, 2006

Contents

List of Figures

List of Tables

Summary

This thesis deals with coordinated position control of satellite formations. Both a linear and nonlinear model for the position dynamics of a spacecraft formation are presented for a Leader/Follower architecture. A passivity-based controller is derived to control the satellites during formation flying maneuvers and to compensate for perturbations, such as the J_2-effect. The Hill-Clohessy-Wiltshire equations are used to derive fuel efficient paths appropriate for satellite formations in orbit around the Earth.

Two relevant cases are investigated to see how they fit into the framework of hybrid systems, namely the spacecraft formation flying problem and the use of thrusters as actuators for satellites in formation. The theory of hybrid systems is presented and the concept of mode switching is applied to the above cases. Simulations are performed in MATLAB Simulink and the Stateflow environment to show the use of the hybrid control approach. It is concluded that both the formation flying problem and the proposed thruster control system benefit from adoption of the hybrid paradigm.

Chapter 1

Introduction

Spacecraft formation flying guidance and control has drawn a considerable amount of research efforts. An overview of the research done in this field is given in Scharf, Hadaegh & Ploen (2003) and Scharf, Hadaegh & Ploen (2004). In order to maintain the satellite formation over a long period of time, a control system must be designed to compensate for the deviation of the motion of the satellites from the desired trajectories. A global control law that must satisfy the requirements of a multi-agent, multi-objective formation for the entire lifetime of the mission might be difficult, if not impossible, to design. Instead, it might be attractive to model the desired maneuvers as modes of operation, where each mode has its own continuous dynamical laws, with a discrete logic that controls the switching between these modes. This type of dynamical system, which combines continuous and discrete components, is denoted as a hybrid system.

Spacecraft flying in formation often have several mission objectives to complete. Science missions such as optical interferometry, Earth and Solar observation often require the satellites to perform different formation flying maneuvers, such as geometrical reconfigurations. Formation flying is therefore a relevant application for adopting a hybrid control approach.

1.1 Contributions of this thesis

The contributions of this thesis are as follows. First, a nonlinear model for the position dynamics of a Leader/Follower satellite formation is derived, including the J_2-perturbation, which needs to be taken into account. The theory of hybrid system is introduced, as well as several issues and challenges regarding the stability analysis of such a system.

Furthermore, the concept of mode switching is applied to a formation of 4 satellites orbiting the Earth, to see how the satellite formation flying problem fits into the framework of hybrid systems. Several maneuvers, such as geometrical reconfiguration and leader-reassignment, are presented and then simulated for the above system.

In addition, the hybrid paradigm is applied to the thruster control system of a satellite in formation. Simulations in MATLAB Simulink and the Stateflow environment show the successful use of a hybrid control approach for the two relevant cases mentioned.

1.2 Outline of the project

Chapter 2 Introduction to Keplerian orbits and basic orbital mechanics.

Chapter 3 Descriptions of reference frames used when describing position and attitude of satellites.

Chapter 4 The notations and mathematical background used throughout the project are described.

Chapter 5 The Hill-Clohessy-Wiltshire equations are presented in this chapter, as well as the relative position dynamics of the satellites. Some satellite formations based on the HCW equations are also introduced.

Chapter 6 An introduction to the perturbations affecting the satellite formation in orbit around the earth, such as the J_2-effect.

Chapter 7 The theory of hybrid systems is introduced, as well as an overview of the research done on stability theory for hybrid systems. Examples are given to clarify the theory.

Chapter 8 In this chapter an introduction to spacecraft propulsion systems is given, together with the theory on thruster modeling and control. The thruster control case mentioned in chapter 7.4 is designed and analyzed at the end of the chapter.

Chapter 9 Design and analysis of the supervisory control case for a satellite formation. The passivity-based controller that is used in this thesis is also derived in this chapter, along with an overview of the research done on alternative control schemes.

Chapter 10 Simulation and discussion of the thruster control case and the supervisory control case presented in chapter 8 and 9.

Chapter 11 Conclusions made from the work done in this project are presented, and recommendations for further work are given.

Appendix A Overview of the CD contents.

Chapter 2

Keplerian Orbits

Johannes Kepler deduced three laws that describe planetary motion, which also apply to satellites orbiting the Earth (Wertz & Larson 1999):

First Law The orbit of each planet is an ellipse, with the Sun at one focus

Second Law The line joining the planet to the Sun sweeps out equal areas in equal times

Third Law The square of the period of a planet is proportional to the cube of its mean distance from the Sun

Keplerian orbits and Newton's laws are treated in Sidi (1997) and Wertz & Larson (1999). The two-body problem that is used as a starting point in the derivation the HCW's equations in chapter 5 is obtained from these laws. They provide the basis for most analysis of satellite orbit dynamics. The key parameters of an elliptic orbit around the Earth is depicted in Figure 2.1, and described in Table 2.1.

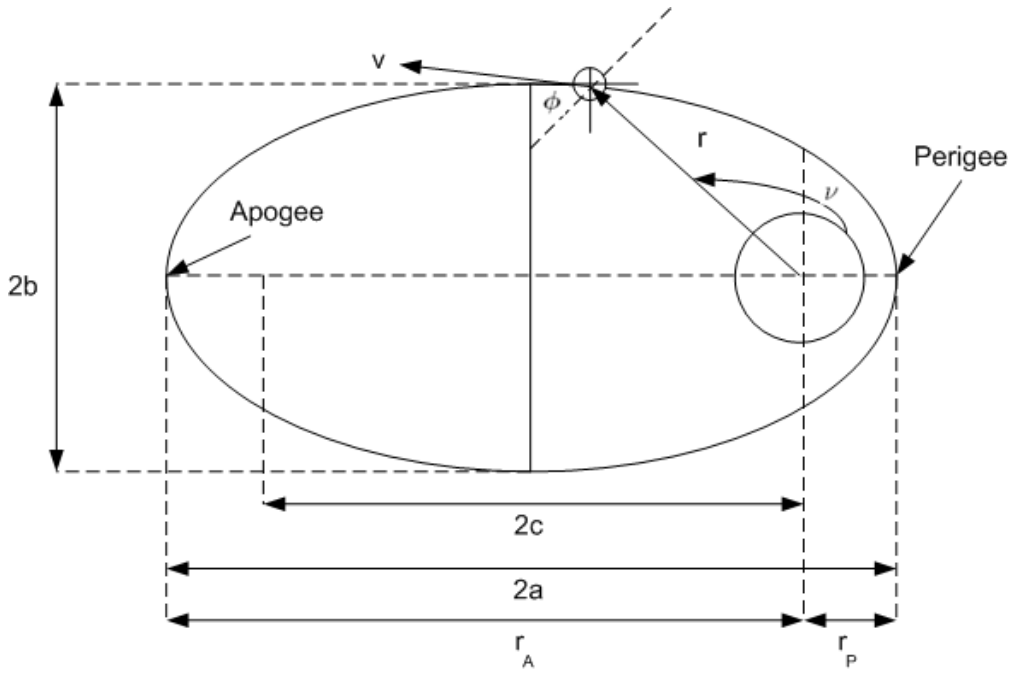

Figure 2.1: Geometry of an elliptic orbit (Wertz & Larson 1999)

r	position vector of the satellite relative to Earth's center
V	velocity vector of the satellite relative to Earth's center
$\boldsymbol{\phi}$	*flight-path-angle*, the angle between the velocity vector and a line perpendicular to the position vector
a:	semimajor axis of the ellipse
b:	semiminor axis of the ellipse
c:	the distance from the center of the orbit to one of the focii
ν :	the *true anomaly*, the polar angle of the ellipse
r_A:	*radius of apogee*, the distance from Earth's center to the farthest point on the ellipse
r_P:	*raidus of perigee*, the distance from Earth's center to the point of closest approach to the Earth

Table 2.1: Parameters of an elliptical orbit (Wertz & Larson 1999)

Chapter 3

Reference Frames

When representing position and attitude for satellites in 6 *degrees of freedom* (DOF), the following reference frames are convenient, see Fossen (2002).

3.1 Earth-Centered Inertial Frame

The Earth-Centered Inertial frame (ECI) is a non-accelerating reference frame in which Newton's laws of motion apply. The origin of the ECI coordinate frame $x_i y_i z_i$ is located at the center of the Earth.

3.2 Earth-Centered Earth-Fixed Frame

The Earth-Centered Earth-Fixed frame (ECEF) $x_e y_e z_e$ has its origin fixed to the center of the Earth, but the axes rotate relative to the inertial frame ECI, which is fixed in space. The angular rate of rotation is $\omega_e = 7.2921 \cdot 10^{-5}$ rad/s.

3.3 Body Frame

The body-fixed reference frame $x_b y_b z_b$ is a moving coordinate frame which is fixed to the satellite. The position and orientation of the satellite are described relative to the ECI frame, while the linear and angular velocities should be expressed in the body-fixed coordinate system. The body axes x_b, y_b and z_b are chosen to coincide with the *principal axes of inertia.*

The reference frames mentioned above are shown in Figure 3.1.

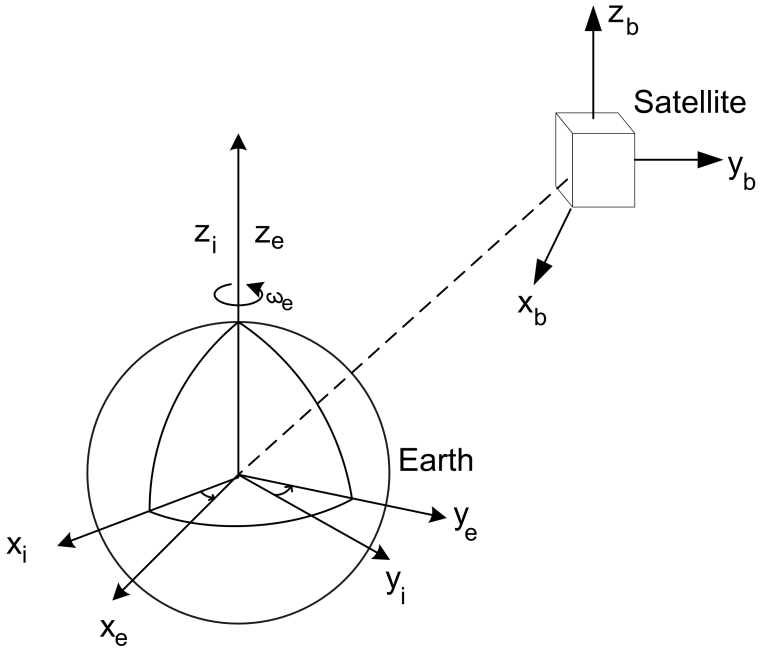

Figure 3.1: Reference frames

Chapter 4

Mathematical Notation and Background

This chapter presents the definitions and notation used throughout this thesis. The material is taken from Fossen (2002) and Egeland & Gravdahl (2002).

4.1 Vectors

A vector $\vec{u}$ can be described by its magnitude $|\vec{u}|$ and its direction. This description of a vector does not rely on the definition of any coordinate frame, and can in this respect be said to be *coordinate-free*. Two alternative vector representations can be described by introducing the Cartesian coordinate frame (Egeland & Gravdahl 2002).

The vector $\vec{u}$ can be expressed as a linear combination of the orthogonal unit vectors $\vec{a_1}, \vec{a_2}$ and $\vec{a_3}$ of the Cartesian coordinate frame a:

$$\vec{u} = u_1\vec{a_1} + u_2\vec{a_2} + u_3\vec{a_3} \tag{4.1}$$

where

$$\vec{u_i} = \vec{u} \cdot \vec{a_i}, \quad i \in \{1, 2, 3\} \tag{4.2}$$

are the unique *components* or *coordinates* of $\vec{u}$ in a.

The second vector representation is the *coordinate vector* form where the coordinates of the vectors are written as a column vector:

$$\mathbf{u}^a = \begin{bmatrix} u_1^a \\ u_2^a \\ u_3^a \end{bmatrix} \quad , \quad \mathbf{u}^b = \begin{bmatrix} u_1^b \\ u_2^b \\ u_3^b \end{bmatrix} \tag{4.3}$$

where superscript a denotes that the vector is given by the coordinates in a, and the superscript b denotes that the vector is given by the coordinates in b. The latter representation will be used in this dissertation.

4.2 Rotation Matrices

The coordinate transformation from frame b to a is given by (Egeland & Gravdahl 2002):

$$\mathbf{v}^a = \mathbf{R}_b^a \mathbf{v}^b \tag{4.4}$$

where

$$\mathbf{R}_b^a = \{\vec{a_i} \cdot \vec{b_j}\} \tag{4.5}$$

is called the *rotation matrix* from a to b. The elements $r_{ij} = \vec{a_i} \cdot \vec{b_j}$ of the rotation matrix R_b^a are called the *direction cosines*.

4.2.1 Properties of the Rotation Matrix

The transformation from frame a to b can be found by interchanging a and b in the expressions. This gives:

$$\mathbf{R}_a^b = \{\vec{b_i} \cdot \vec{a_j}\} \tag{4.6}$$

For all $\mathbf{v}^b$ we have

$$\mathbf{v}^b = \mathbf{R}_a^b \mathbf{v}^a = \mathbf{R}_a^b \mathbf{R}_b^a \mathbf{v}^b \tag{4.7}$$

This implies that:

$$\mathbf{R}_a^b \mathbf{R}_b^a = \mathbf{I}, \tag{4.8}$$

the property of rotation matrices called orthonormality. And it follows that:

$$\mathbf{R}_a^b = (\mathbf{R}_b^a)^{-1} \tag{4.9}$$

A comparison of the elements in the matrices in (4.5) and (4.6) leads to the conclusion that $\mathbf{R}_a^b = (\mathbf{R}_b^a)^T$. Combining these results gives:

$$\mathbf{R}_a^b = (\mathbf{R}_b^a)^{-1} = (\mathbf{R}_b^a)^T \tag{4.10}$$

Time differentiation of the matrix product:

$$\frac{d}{dt}\left[\mathbf{R}_b^a (\mathbf{R}_b^a)^T\right] = \dot{\mathbf{R}}_b^a (\mathbf{R}_b^a)^T + \mathbf{R}_b^a (\dot{\mathbf{R}}_b^a)^T = \mathbf{0} \tag{4.11}$$

By defining:

$$\mathbf{S} = \dot{\mathbf{R}}_b^a (\mathbf{R}_b^a)^T \tag{4.12}$$

we get from (4.11) that $\mathbf{S} + \mathbf{S}^T = \mathbf{0}$ which implies that the matrix:

$$\mathbf{S} = \dot{\mathbf{R}}_b^a (\mathbf{R}_b^a)^T = -\dot{\mathbf{R}}_b^a (\mathbf{R}_b^a)^T = -\mathbf{S}^T \tag{4.13}$$

is *skew symmetric*.

Let the vector $\vec{\omega_{ab}}$ be defined by requiring that its coordinate form $\boldsymbol{\omega}_{ab}^a$ in frame a satisfies:

$$(\boldsymbol{\omega}_{ab}^a)^\times = \dot{\mathbf{R}}_b^a (\mathbf{R}_b^a)^T = \mathbf{S}(\boldsymbol{\omega}_{ab}^a) \tag{4.14}$$

where $\vec{\omega}_{ab}$ is said to be the *angular velocity* vector of frame b relative to frame a.

The vector cross product $\times$ is defined by (Fossen 2002):

$$\boldsymbol{\lambda} \times \mathbf{a} := \mathbf{S}(\boldsymbol{\lambda})\mathbf{a} \tag{4.15}$$

where

$$\mathbf{S}(\boldsymbol{\lambda}) = \mathbf{S}^T(\boldsymbol{\lambda}) = \begin{bmatrix} 0 & -\lambda_3 & \lambda_2 \\ \lambda_3 & 0 & -\lambda_1 \\ -\lambda_2 & \lambda_1 & 0 \end{bmatrix}, \ \boldsymbol{\lambda} = \begin{bmatrix} \lambda_1 \\ \lambda_2 \\ \lambda_3 \end{bmatrix} \tag{4.16}$$

This implies that:

$$\mathbf{S}(\boldsymbol{\omega}_{ab}^a) = \begin{bmatrix} 0 & -\omega_z & \omega_y \\ \omega_z & 0 & -\omega_x \\ -\omega_y & \omega_x & 0 \end{bmatrix} \tag{4.17}$$

The kinematic differential equation of the rotation matrix can be given by the two alternative forms:

$$\dot{\mathbf{R}}_b^a = (\boldsymbol{\omega}_{ab}^a)^\times \mathbf{R}_b^a \tag{4.18}$$

$$\dot{\mathbf{R}}_b^a = \mathbf{R}_b^a (\boldsymbol{\omega}_{ab}^b)^\times \tag{4.19}$$

where (4.18) is obtained by post-multiplication of (4.14) with $\mathbf{R}_b^a$, and (4.19) by using the coordinate transformation rule $(\boldsymbol{\omega}_{ab}^a)^\times = \mathbf{R}_b^a (\boldsymbol{\omega}_{ab}^a)^\times \mathbf{R}_a^b$ for the skew symmetric form of a vector.

The rotation matrix $\mathbf{R}_b^a$ from a to b has two interpretations, according to Egeland & Gravdahl (2002). It can act as a coordinate transformation matrix, by transforming $\mathbf{v}^b$ to $\mathbf{v}^a$, as shown in (4.4), and it can act as a rotation matrix. In the latter case $\mathbf{R}_b^a$ rotates a vector $\vec{p}$, with coordinate vector $\mathbf{p}^a$ in a, to the vector $\vec{q}$, with coordinate vector $\mathbf{q}^b = \mathbf{p}^a$, by:

$$\mathbf{q}^a = \mathbf{R}_b^a \mathbf{p}^a \tag{4.20}$$

The determinant of the rotation matrix $\mathbf{R}_b^a$ is found by direct calculation to be equal to unity:

$$\det \mathbf{R}_b^a = 1 \tag{4.21}$$

The rotation matrix $\mathbf{R}$ between two frames a and b is denoted as $\mathbf{R}_b^a$, and it is an element in the set $SO(3)$, that is the special orthogonal group of order 3:

$$SO(3) = \{\mathbf{R} | \mathbf{R} \in R^{3\times 3},\ \mathbf{R}^T\mathbf{R} = \mathbf{I} \text{ and } \det\mathbf{R} = 1\} \tag{4.22}$$

4.2.2 Simple Rotations

A rotation about a fixed axis is called a *simple rotation*. The rotation matrices corresponding to simple rotations about the x, y and z axes are:

$$\mathbf{R}_x(\phi) = \begin{bmatrix} 1 & 0 & 0 \\ 0 & \cos\phi & -\sin\phi \\ 0 & \sin\phi & \cos\phi \end{bmatrix} \tag{4.23}$$

$$\mathbf{R}_y(\theta) = \begin{bmatrix} \cos\theta & 0 & \sin\theta \\ 0 & 1 & 0 \\ -\sin\theta & 0 & \cos\theta \end{bmatrix} \tag{4.24}$$

$$\mathbf{R}_z(\psi) = \begin{bmatrix} \cos\psi & -\sin\psi & 0 \\ \sin\psi & \cos\psi & 0 \\ 0 & 0 & 1 \end{bmatrix} \tag{4.25}$$

4.2.3 Composite Rotations

The rotation from frame a to a frame c may be described as a *composite rotation* made up by a rotation from a to b, and then from b to c. The rotation matrix of a composite rotation is (Egeland & Gravdahl 2002):

$$\mathbf{R}_c^a = \mathbf{R}_b^a\mathbf{R}_c^b \tag{4.26}$$

Chapter 5

Equations of Motion

In this chapter the Hill-Clohessy-Wiltshire equations (Clohessy & Wiltshire 1960) will be presented. The equations are deduced under the assumptions that the Earth is a perfect sphere, and that the Leader satellite is in a Keplerian circular orbit. After deriving the unperturbed HCW's equations, the equations will be generalized to include perturbations, resulting in a nonlinear model for the position of a Follower satellite relative to the Leader satellite.

5.1 The Hill-Clohessy-Wiltshire Equations

Most of the material in this section is taken from Schwartz (2004) and Grøtli (2005). The HCW's equations describe the motion of a follower spacecraft relative to a leader spacecraft. For a satellite orbiting the Earth, the two-body problem applies, under the assumptions that:

1. The equations of motion are expressed in a non-inertial reference frame whose origin coincides with the center of mass of the central body.
2. Both the central body and satellite are homogenous spheres or points of equivalent mass.
3. The inverse-square gravitational force between the two bodies is the only force in action.

The governing equation is then

$$\ddot{\vec{r}}_i = -\frac{G(M+m)}{r_i^3}\vec{r}_i \; ; \quad i = l, f \tag{5.1}$$

where G is the gravitational constant, M is the mass of the central body, m_i is the mass of the satellite in question, $\vec{r}_i$ is the vector from the center of mass of the central body to the satellite, and $i = l, f$ denote the Leader and Follower satellite, respectively.

It is convenient to express the relative motion equations in a circular reference frame, called the Hill frame. The Hill frame rotates once per orbit with respect to the inertial frame. The axes of the Hill frame, $\vec{e}_r$, $\vec{e}_\theta$ and $\vec{e}_z$ are defined in the radial, velocity, and orbit-normal directions, respectively. The angular velocity of the rotating reference frame is given by:

$$\vec{\omega}_{ih} = \dot{\nu}\vec{e_z} \tag{5.2}$$

where ν is the true anomaly of the Leader satellite's orbit. The position vector for the Follower satellite with respect to the Leader is then given by:

$$\vec{\rho} = \vec{r_f} - \vec{r_l} \tag{5.3}$$

which can be expressed as:

$$\vec{\rho} = x\vec{e_r} + y\vec{e_\theta} + z\vec{e_z} \tag{5.4}$$

where x, y and z are the components of $\vec{\rho}$ in the Hill frame, see Figure 5.1.

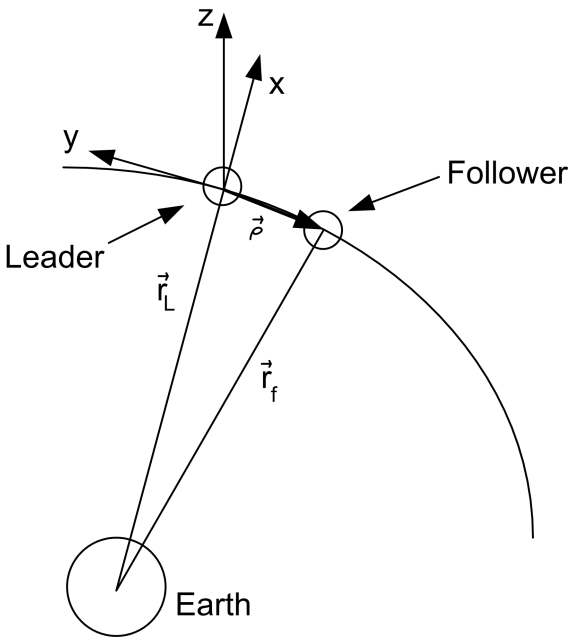

Figure 5.1: Hill frame

The second derivative of $\vec{\rho}$ yields:

$$\ddot{\vec{\rho}} = \ddot{x}\vec{e_r} + 2\dot{x}\dot{\vec{e_r}} + x\ddot{\vec{e_r}} + \ddot{y}\vec{e_\theta} + 2\dot{y}\dot{\vec{e_\theta}} + y\ddot{\vec{e_\theta}} + \ddot{z}\vec{e_z} \tag{5.5}$$

Inserting for the time derivatives $\dot{\vec{e_r}}$, $\ddot{\vec{e_r}}$, $\dot{\vec{e_\theta}}$ and $\ddot{\vec{e_\theta}}$ gives:

$$\begin{aligned}\ddot{\vec{\rho}} &= \ddot{x}\vec{e_r} + 2\dot{x}\dot{\nu}\vec{e_\theta} - x\dot{\nu}^2\vec{e_r} + x\ddot{\nu}\vec{e_\theta} + \ddot{y}\vec{e_\theta} - 2\dot{y}\dot{\nu}\vec{e_r} - y\dot{\nu}^2\vec{e_\theta} - y\ddot{\nu}\vec{e_r} + \ddot{z}\vec{e_z} \\ &= (\ddot{x} - 2\dot{y}\dot{\nu} - x\dot{\nu}^2 - y\ddot{\nu})\vec{e_r} + (\ddot{y} + 2\dot{x}\dot{\nu} - y\dot{\nu}^2 + x\ddot{\nu})\vec{e_\theta} + \ddot{z}\vec{e_z}\end{aligned} \tag{5.6}$$

The specific angular momentum is defined as:

$$\vec{h} \equiv \frac{\vec{L}}{m} \equiv \frac{\vec{r} \times \vec{p}}{m} = \vec{r} \times \dot{\vec{r}} \tag{5.7}$$

Using polar coordinates and the relation $\dot{\vec{e}}_r = \dot{\theta}\vec{e}_\theta$ for the specific angular momentum of the Leader satellite gives:

$$\begin{aligned}\vec{h_l} &= \vec{r_l} \times \dot{\vec{r_l}} \\ &= r_l\vec{e_r} \times (\dot{r}\vec{e_r} + r_l\dot{\vec{e_r}}) \\ &= r_l\vec{e_r} \times (\dot{r}\vec{e_r} + r_l\dot{\nu}\vec{e_\theta}) \\ &= r_l^2\dot{\nu}\vec{e_z}\end{aligned} \tag{5.8}$$

Differentiating the specific angular momentum for the Leader satellite, using (5.1) for $\ddot{\vec{r_l}}$, yields:

$$\begin{aligned}\dot{\vec{h_l}} &= \dot{\vec{r_l}} \times \dot{\vec{r_l}} + \vec{r_l} \times \ddot{\vec{r_l}} \\ &= \vec{0} + \vec{r_l} \times (-\frac{G(M+m_l)}{r_l^3}\vec{r_l}) \\ &= -\frac{G(M+m_l)}{r_l^3}\vec{r_l} \times \vec{r_l} \\ &= \vec{0}\end{aligned} \tag{5.9}$$

Thus $\vec{h_l}$ is conserved. Since $h_l = r_l^2\dot{\nu}$ is constant we have that

$$\dot{h_l} = 2r_l\dot{r_l}\dot{\nu} + r_l^2\ddot{\nu} = r_l(2\dot{r_l}\dot{\nu} + r_l\ddot{\nu}) = 0 \tag{5.10}$$

This provides a constraint on the second derivative of the true anomaly of the Leader satellite's orbit:

$$\ddot{\nu} = -2\frac{\dot{r_l}}{r_l}\dot{\nu} \tag{5.11}$$

Using that $\vec{r_l} = \vec{r_f} + \vec{\rho}$, given in (5.3), and the same procedure that was used to find $\ddot{\vec{\rho}}$ in (5.6), the Leader satellite's acceleration equation can now be written as:

$$\begin{aligned}\ddot{\vec{r_l}} &= (\ddot{r_l} - r_l\dot{\nu}^2)\vec{e_r} + (2\dot{r_l}\dot{\nu} + r_l\ddot{\nu})\vec{e_\theta} \\ &= (\ddot{r_l} - r_l\dot{\nu}^2)\vec{e_r}\end{aligned} \tag{5.12}$$

Maintaining the assumption that there are no perturbations, (5.1) is compared with (5.12), which gives the following scalar equation for the acceleration for the Leader satellite:

$$\ddot{r_l} = r_l\dot{\nu}^2 - \frac{G(M+m_l}{r_l^2} = r_l\dot{\nu}^2 - \frac{\mu}{r_l^2} \tag{5.13}$$

where $\mu = GM \approx G(M+m_{l,f})$, since $M >> m_{l,f}$. The acceleration equation of the Follower satellite can similarily be obtained, using (5.3) and polar coordinates:

$$\begin{aligned}\ddot{\vec{r_f}} = &((r_l\dot{\nu}^2 - \frac{\mu}{r_l^2}) + \ddot{x} - 2\dot{y}\dot{\nu} - \ddot{\nu}y - \dot{\nu}^2(r_l+x))\vec{e_r} \\ &+ (\ddot{y} + 2\dot{\nu}(\dot{r_l}+\dot{x}) + \ddot{\nu}(r_l+x) - y\dot{\nu}^2)\vec{e}_\theta \\ &+ \ddot{z}\vec{e}_z\end{aligned} \tag{5.14}$$

By using (5.1), (5.11) and (5.13) for $\ddot{\vec{r}}_f$, $\ddot{\nu}$ and $\ddot{r}_l$, respectively, equation (5.14) can be rewritten as:

$$\begin{aligned}\ddot{\vec{r_f}} &= ((r_l\dot{\nu}^2 - \frac{\mu}{r_l^2}) + \ddot{x} - 2\dot{y}\dot{\nu} - (-2\frac{\dot{r_l}}{r_l}\dot{\nu})y - \dot{\nu}^2(r_l+x))\vec{e_r} \\ &\quad + (\ddot{y} + 2\dot{\nu}(\dot{r_l}+\dot{x}) + (-2\frac{\dot{r_l}}{r_l}\dot{\nu})(r_l+x) - y\dot{\nu}^2)\vec{e}_\theta \\ &\quad + \ddot{z}\vec{e}_z \\ &= (\ddot{x} - 2\dot{\nu}(\dot{y} - y\frac{\dot{r_l}}{r_l}) - x\dot{\nu}^2 - \frac{\mu}{r_l^2})\vec{e_r} \\ &\quad + (\ddot{y} + 2\dot{\nu}(\dot{x} - x\frac{\dot{r_l}}{r_l}) - y\dot{\nu}^2)\vec{e}_\theta \\ &\quad + \ddot{z}\vec{e}_z \\ &= -\frac{\mu}{r_f^3}\vec{r_f}\end{aligned} \tag{5.15}$$

This vector expression can be written as three scalar equations:

$$\ddot{x} - 2\dot{\nu}(\dot{y} - y\frac{\dot{r_l}}{r_l}) - x\dot{\nu}^2 - \frac{\mu}{r_l^2} = -\frac{\mu}{r_f^3}(r_l+x) \tag{5.16a}$$

$$\ddot{y} + 2\dot{\nu}(\dot{x} - x\frac{\dot{r_l}}{r_l}) - y\dot{\nu}^2 = -\frac{\mu}{r_f^3}y \tag{5.16b}$$

$$-\ddot{z} = -\frac{\mu}{r_f^3}z \tag{5.16c}$$

which are the full, nonlinear equations of relative motion for a Follower spacecraft with respect to a Leader spacecraft in an unperturbed orbit.

From basic orbital dynamics we have that (Wie 1998):

$$r = \frac{p}{1 + e\cos\nu} \tag{5.17}$$

where ν is called the *true anomaly*, e is the eccentricity of the orbit and p, called the parameter or *semilatus rectum*, is defined as:

$$p = h^2/\mu \tag{5.18}$$

Equation (5.17) is the equation of a conic section, written in terms of polar coordinates r and ν with the origin located at a focus, whereas ν is measured from the point on the conic nearest the focus. This equation is a statement of Kepler's first law (Wie 1998). The size of the conic section is determined by p and its shape is determined by the eccentricity e.

The rate of the true anomaly of the Leader satellite is given as (Kristiansen, Loria, Chaillet & Nicklasson 2006):

$$\dot{\nu} = \frac{n(1 + ecos\nu)^2}{(1 - e^2)^3} \tag{5.19}$$

where $n = \sqrt{\mu/a_l^3}$ is the mean motion of the leader, and a_l is the semimajor axis of the leader orbit. Differentiation of (5.19) yields (Kristiansen et al. 2006):

$$\ddot{\nu} = \frac{-2n^2 e(1 + ecos\nu)^3 sin\nu}{(1 - e^2)^3} \tag{5.20}$$

Equations (5.19) and (5.20) are useful when modeling a satellite formation that revolves around the Earth in an elliptical orbit.

Inserting (5.17) into $h_l = r_l^2\dot{\nu}$ yields:

$$h_l = r_l^2\dot{\nu} = \frac{p^2}{(1 + e\text{cos}\nu)^2}\dot{\nu} \tag{5.21}$$

This equation can be rewritten as:

$$\frac{\dot{\nu}^2}{1 + e\text{cos}\nu} = \frac{h_l\dot{\nu}(1 + e\text{cos}\nu)}{p^2} = \frac{\mu}{r_l^3} \tag{5.22}$$

Assuming a Keplerian circular orbit the change-in-radius, $\dot{r}_l$, and the eccentricity terms drop out, and the derivative of the true anomaly, $\dot{\nu}$, can be replaced by the mean motion, n. For a close formation $r_l \approx r_f$, which can be justified by the following:

$$\begin{aligned} r_f &= \sqrt{(r_l + x)^2 + y^2 + z^2} \\ &= r_l\sqrt{1 + \frac{2x}{r_l} + \frac{x^2 + y^2 + z^2}{r_l^2}} \\ &\approx r_l\sqrt{1 + \frac{2x}{r_l}} \end{aligned} \tag{5.23}$$

By making use of these substitutions in (5.16a), (5.16b) and (5.16c) we obtain the unperturbed Hill-Clohessy-Wiltshire (HCW) equations:

$$\ddot{x} - 2n\dot{y} - 3n^2x = 0 \tag{5.24a}$$

$$\ddot{y} + 2n\dot{x} = 0 \tag{5.24b}$$

$$\ddot{z} + n^2z = 0 \tag{5.24c}$$

These linearized equations of motion are useful in describing the relative orbital dynamics in spacecraft formation flight. The unperturbed HCW equations in (5.24a), (5.24b) and (5.24c) can be solved analytically:

$$x(t) = \frac{\dot{x}_0}{n}\mathrm{sin}nt - (3x_0 + 2\frac{\dot{y}_0}{n})\mathrm{cos}nt + 4x_0 + 2\frac{\dot{y}_0}{n} \tag{5.25a}$$

$$y(t) = \frac{2\dot{x}_0}{n}\mathrm{cos}nt + (6x_0 + 4\frac{\dot{y}_0}{n})\mathrm{sin}nt - (6nx_0 + 3\dot{y}_0)t - \frac{2x_0}{n} + y_0 \tag{5.25b}$$

$$z(t) = \frac{\dot{z}_0}{n}\mathrm{sin}nt + z_0\mathrm{cos}nt \tag{5.25c}$$

Equation (5.25b) includes a secular term, i.e. a term that increases linearly in time. To eliminate the secular drift the following additional constraint is invoked:

$$\dot{y}_0 = -2x_0n \tag{5.26}$$

Invoking this constraint results in a relative orbit that is displaced from, but has the same energy, and thus the same semimajor axis, as the reference orbit, which leads to:

$$x(t) = \frac{\dot{x}_0}{n}\mathrm{sin}nt + x_0\mathrm{cos}nt \tag{5.27a}$$

$$y(t) = \frac{2\dot{x}_0}{n}\mathrm{cos}nt - 2x_0\mathrm{sin}nt - \frac{2\dot{x}_0}{n} + y_0 \tag{5.27b}$$

$$z(t) = \frac{\dot{z}_0}{n}\mathrm{sin}nt + z_0\mathrm{cos}nt \tag{5.27c}$$

5.2 Relative Position Dynamics

The nonlinear model for the Leader/Follower relative position case will now be derived. Generalizing equation (5.1) gives:

$$\ddot{\vec{r}}_i = -\frac{G(M+m)}{r_i^3}\vec{r}_i - \frac{\vec{F}_{di}}{m_i} + \frac{u_i}{m_i}\ ; \quad i = l, f \tag{5.28}$$

where the forcing terms due to disturbances, $F_{dl,df} \in \Re^3$, and the control input vectors $u_{l,f} \in \Re^3$, have been included. By using (5.28) and the relation $\vec{\rho} = \vec{r_f} - \vec{r_l}$, the relative position dynamics can be obtained (Yan, Yang, Kapila & de Queiroz 2000):

$$m_f\ddot{\vec{\rho}} + m_f\mu\left(\frac{\vec{r_l} + \vec{\rho}}{(r_l + \rho)^3} - \frac{\vec{r_l}}{r_l^3}\right) + \frac{m_f}{m_l}\vec{u}_l + \vec{F}_{df} - \frac{m_f}{m_l}\vec{F}_{dl} = \vec{u}_f \tag{5.29}$$

This equation can be rewritten, by the use of (5.6), on the following advantageous form (Yan, Yang, Kapila & de Queiroz 2000):

$$\mathbf{M}\ddot{\boldsymbol{\rho}} + \boldsymbol{C}(\dot{\nu}, m_f)\dot{\boldsymbol{\rho}} + \mathbf{n}(\boldsymbol{\rho}, \dot{\nu}, \ddot{\nu}, r_l) + \frac{m_f}{m_l}\boldsymbol{u}_l + \boldsymbol{F}_d = \boldsymbol{u}_f \tag{5.30}$$

where

$$\boldsymbol{F}_d = \boldsymbol{F}_{df} - \frac{m_f}{m_l}\boldsymbol{F}_{dl} \tag{5.31}$$

is the composite disturbance force,

$$\boldsymbol{\rho} = \begin{bmatrix} x(t) \\ y(t) \\ z(t) \end{bmatrix} \tag{5.32}$$

is the relative position vector,

$$\boldsymbol{C}(\dot{\nu}, m_f) = 2m_f\dot{\nu}\begin{bmatrix} 0 & -1 & 0 \\ 1 & 0 & 0 \\ 0 & 0 & 0 \end{bmatrix} \tag{5.33}$$

is the Coriolis-like matrix,

$$\boldsymbol{M} = \begin{bmatrix} m_f & 0 & 0 \\ 0 & m_f & 0 \\ 0 & 0 & m_f \end{bmatrix} \tag{5.34}$$

is the Mass matrix and

$$\boldsymbol{n}(\boldsymbol{\rho}, \dot{\nu}, \ddot{\nu}, r_l) = m_f \begin{bmatrix} \mu(\frac{r_l+x}{r_f^3} - \frac{1}{r_l^2}) - (\dot{\nu}^2 x + \ddot{\nu} y) \\ \mu(\frac{y}{r_f^3}) - (y\dot{\nu}^2 - \ddot{\nu} x) \\ \mu(\frac{z}{r_f^3} \end{bmatrix} \tag{5.35}$$

is a nonlinear term. Equation (5.30) represents the same equations as (5.16a-c), but with forcing terms included. This matrix form of the equations of motion resemble the dynamic models of robot manipulators and marine vehicles, see for example Sciavicco & Siciliano (2005) and Fossen (2002), implying that known control methods developed for those types of mechanical agents might also be used for the control of satellite formations (Grøtli 2005).

The use of this similarity to derive controllers for satellite formations architecture has been done by Grøtli (2005) for continuous position control of a Leader/Follower architecture modeled by (5.30). The theory used was a passivity-based approach found in Berghuis & Nijmeijer (1993). The same has been done for the attitude case in Krogstad (2005), where theory based on synchronization of mechanical systems, e.g. robots and ships, is applied to satellites actuated by means of four reaction wheels in a tetrahedron configuration. The latter was done for satellites modeled as rigid bodies, and was based on two control schemes from Rodriguez-Angeles (2002).

5.3 Satellite Formations

The HCW equations yield several fuel efficient paths for the satellite formation, including along-track, in-plane, circular and projected formations. For the along-track formation both satellites are in the same orbital plane, only separated by a difference in time. In this formation the Follower satellite has the same desired trajectory as the leader satellite, except for a y displacement, which yields a constant offset in the along-track direction (Schwartz 2004). Special cases of satellite formations are treated in Yeh & Sparks (2000). In this thesis the along-track formation will be used for a Leader/Follower architecture. The Leader/Follower approach and other formation flying architectures are described in chapter 9.1.

Chapter 6

Perturbations

In the previous chapter, the HCW equations for relative motion in an orbit for a Leader/-Follower architecture were presented. The HCW equations are used to model the Follower satellite's relative motion with respect to the Leader satellite. These equations are also essential in the design of tracking controllers, to herd the member satellites into a desired formation after the initial deployment, and to nudge them back into formation as soon as they start drifting due to perturbations (Yeh & Sparks 2000).

Perturbations such as the J_2-effect due to the oblateness of the Earth, atmospheric drag, solar radiation and solar wind will cause the orbits of the satellite formation to deteriorate over time, showing the need for a control system that takes model perturbations and disturbances into consideration.

With the assumption of a close formation, the perturbation due to the J_2-effect on the relative motion is the difference between that of the Follower satellite and that of the Leader satellite. The net result is therefore greatly reduced. Furthermore, if the Leader and Follower satellites are assumed to be identical copies with the same reflectivities, the net perturbation due to solar radiation and atmospheric drag are also greatly reduced (Yeh & Sparks 2000).

6.1 Gravitational J_2 Perturbation

Due to the inhomogeneous distribution of mass of the primary body, the Earth, the assumption that the total mass of the Earth is concentrated in the center of the coordinate system, and the gravitational law (5.1),

$$\ddot{\vec{r}} = -\frac{\mu}{r^3}\vec{r}$$

where $\mu = GM$, might not be satisfactory. For precise orbit determination, it is necessary to take into account the higher order variations in the gravitational potential of the Earth. A more realistic model can be found in Montenbruck & Gill (2000), and will be given here for

the sake of completeness. An equivalent representation of (5.1) is given as:

$$\ddot{\vec{r}} = \nabla U \quad \text{with} \quad U = \frac{\mu}{r} \tag{6.1}$$

where U is called the gravity potential. This expression can be generalized to an arbitrary mass distribution by summing up the contributions from each of the mass elements $dm = \rho(\vec{s})d^3\vec{s}$:

$$U = G \int \frac{\rho(\vec{s})d^3\vec{s}}{|\vec{r} - \vec{s}|} \tag{6.2}$$

where $\rho(\vec{s})$ is the density at some point $\vec{s}$ inside the Earth. The inverse of the distance $|\vec{r} - \vec{s}|$ from the satellite to this point $\vec{s}$ can be expanded in a series of Legendre polynomials:

$$\frac{1}{|\vec{r} - \vec{s}|} = \frac{1}{r} \sum_{n=0}^{\infty} \left(\frac{s}{r}\right)^n P_n(\cos\gamma) \quad \text{with} \quad \cos\gamma = \frac{\vec{r} \cdot \vec{s}}{rs} \tag{6.3}$$

where γ is the angle between $\vec{r}$ and $\vec{s}$, and $P_n(u)$ is the Legendre polynomial of degree n:

$$P_n(u) = \frac{1}{2^n n!} \frac{d^n}{du^n}(u^2 - 1)^n \tag{6.4}$$

The longitude λ and latitude ϕ of point $\vec{r}$ are given according to:

$$x = r\ \cos\phi\ \cos\lambda \tag{6.5}$$

$$y = r\ \cos\phi\ \sin\lambda \tag{6.6}$$

$$z = r\ \sin\phi \tag{6.7}$$

The corresponding quantities for point $\vec{s}$ are then chosen as λ' and ϕ'. By using the addition theorem of Legendre polynomials,

$$P_n(\cos\gamma) = \sum_{m=0}^{n} k \frac{(n-m)!}{(n+m)!} P_{nm}(\sin\phi) P_{nm}(\sin\phi')\cos(m(\lambda - \lambda')). \tag{6.8}$$

where $k = 1$ when $m = 0$, $k = 2$ when $m \neq 0$, and $P_{nm}(u)$ is the associated Legendre function of the first kind,

$$P_{nm}(u) = 1 - u^2)^{m/2} \frac{d^m}{du^m} P_n(u), \tag{6.9}$$

with degree n and order m. The Earth's gravity potential can now be written as (Montenbruck & Gill 2000):

$$U = \frac{\mu}{r} \sum_{n=0}^{\infty} \sum_{m=0}^{n} \frac{a^n}{r^n} P_{nm}(\sin\phi)(C_{nm}\cos(m\lambda) + S_{nm}\sin(m\lambda)) \tag{6.10}$$

with the unnormalized coefficients:

$$C_{nm} = \frac{k}{M} \frac{(n-m)!}{(n+m)!} \int \frac{s^n}{a^n} P_{nm}(\sin\phi')\cos(m\lambda')\rho(\vec{s})d^3\vec{s} \tag{6.11}$$

and

$$S_{nm} = \frac{k}{M}\frac{(n-m)!}{(n+m)!}\int \frac{s^n}{a^n} P_{nm}(\sin\phi')\sin(m\lambda')\rho(\vec{s})d^3\vec{s} \tag{6.12}$$

which describe the dependence on the Earth's internal mass distribution. The normalized coefficients $\bar{C}_{nm}$ and $\bar{S}_{nm}$ are defined as:

$$\left\{\begin{matrix}\bar{C}_{nm} \\ \bar{S}_{nm}\end{matrix}\right\} = \sqrt{\frac{(n+m)!}{k(2n+1)(n-m)!}}\left\{\begin{matrix}C_{nm} \\ S_{nm}\end{matrix}\right\} \tag{6.13}$$

which are much more uniform in magnitude than the unnormalized coefficients. By making use of $\bar{C}_{nm}$ and $\bar{S}_{nm}$, and the normalized associated Legendre functions,

$$\bar{P}_{nm} = \sqrt{\frac{k(2n+1)(n-m)!}{(n+m)!}} P_{nm} \ , \tag{6.14}$$

(6.1) may be rewritten as:

$$\ddot{\vec{r}} = \nabla\frac{\mu}{r}\sum_{n=0}^{\infty}\sum_{m=0}^{n}\frac{a^n}{r^n}\bar{P}_{nm}(\sin\phi)(\bar{C}_{nm}\cos(m\lambda) + \bar{S}_{nm}\sin(m\lambda)) \tag{6.15}$$

By the use of several recurrence relations for the evaluation of Legendre polynomials, the Earth's gravity potential at a given point can be derived. The polynomials P_{mm}, with $P_{00} = 1$, are first found from:

$$P_{mm}(u) = (2m-1)(1-u^2)^{1/2}P_{m-1,m-1} \tag{6.16}$$

The remaining values are calculated by using:

$$P_{m+1,m}(u) = (2m+1)uP_{mm}(u) \tag{6.17}$$

and for $n > m+1$ the following relation is used:

$$P_{nm}(u) = \frac{1}{n-m}((2n-1)uP_{n-1,m}(u) - (n+m-1)P_{n-2,m}(u)) \tag{6.18}$$

The gravity potential at a given point may now be written as :

$$U = \frac{\mu}{a}\sum_{n=0}^{\infty}\sum_{m=0}^{n}(C_{nm}V_{nm} + S_{nm}W_{nm}) \tag{6.19}$$

where V_{nm} and W_{nm} are defined as:

$$V_{nm} = \left(\frac{a}{r}\right)^{n+1} P_{nm}(\sin\phi)\cos m\lambda \tag{6.20}$$

$$W_{nm} = \left(\frac{a}{r}\right)^{n+1} P_{nm}(\sin\phi)\sin m\lambda \tag{6.21}$$

Equations (6.20) and (6.21) satisfy the following recurrence relations:

$$V_{mm} = (2m-1)\left(\frac{xa}{r^2}V_{m-1,m-1} - \frac{ya}{r^2}W_{m-1,m-1}\right) \tag{6.22}$$

$$W_{mm} = (2m-1)\left(\frac{xa}{r^2}W_{m-1,m-1} + \frac{ya}{r^2}V_{m-1,m-1}\right) \tag{6.23}$$

and

$$V_{nm} = \left(\frac{2n-1}{n-m}\right)\frac{za}{r^2}V_{n-1,m} - \left(\frac{n+m-1}{n-m}\right)\frac{a^2}{r^2}V_{n-2,m} \tag{6.24}$$

$$W_{nm} = \left(\frac{2n-1}{n-m}\right)\frac{za}{r^2}W_{n-1,m} - \left(\frac{n+m-1}{n-m}\right)\frac{a^2}{r^2}W_{n-2,m} \tag{6.25}$$

where $V_{00} = \frac{a}{r}$, $W_{00} = 0$, $V_{m-1,m} = 0$ and $W_{m-1,m} = 0$. The acceleration $\ddot{\vec{r}} = (\ddot{x}, \ddot{y}, \ddot{z}) = \nabla U$ may now be calculated from (Montenbruck & Gill 2000):

$$\begin{aligned} \ddot{x} &= \sum_{n,m} \ddot{x}_{nm} \\ \ddot{y} &= \sum_{n,m} \ddot{y}_{nm} \\ \ddot{z} &= \sum_{n,m} \ddot{z}_{nm} \end{aligned} \tag{6.26}$$

with the partial accelerations:

$$\begin{aligned} \ddot{x}_{nm} &\overset{(m=0)}{=} \frac{\mu}{a^2}\left(-C_{n0}V_{n+1,1}\right) \\ &\overset{(m>0)}{=} \frac{\mu}{2a^2}\Bigg((-C_{nm}V_{n+1,m+1} - S_{nm}W_{n+1,m+1}) \\ &\quad + \frac{(n-m+2)!}{(n-m)!}(C_{nm}V_{n+1,m-1} + S_{nm}W_{n+1,m-1})\Bigg) \\ \ddot{y}_{nm} &\overset{(m=0)}{=} \frac{\mu}{a^2}\left(-C_{n0}W_{n+1,1}\right) \\ &\overset{(m>0)}{=} \frac{\mu}{2a^2}\Bigg((-C_{nm}W_{n+1,m+1} + S_{nm}V_{n+1,m+1}) \\ &\quad + \frac{(n-m+2)!}{(n-m)!}(C_{nm}W_{n+1,m-1} + S_{nm}V_{n+1,m-1})\Bigg) \\ \ddot{z}_{nm} &\overset{(m\geq 0)}{=} \frac{\mu}{a^2}\Bigg((n-m+1)(-C_{nm}V_{n+1,m} - S_{nm}W_{n+1,m})\Bigg) \end{aligned} \tag{6.27}$$

If one assumes that the mass distribution is symmetric with respect to the axis of rotation, then the expansion of the potential contains only zonal terms, C_{n0}. In addition, the zonal harmonics, when $m = 0$, are symmetric in longitude. Using the notation $J_n = -C_{n0}$ and the

recurrence relations (6.22)-(6.25), the acceleration components in (6.26) can now be found to be:

$$\ddot{x} = -\frac{x_e \mu}{r^3}\left(1 + \frac{3J_2 a^2}{2r^2} - \frac{15J_2 a^2 z_e^2}{2r^4}\right) \tag{6.28}$$

$$\ddot{y} = -\frac{y_e \mu}{r^3}\left(1 + \frac{3J_2 a^2}{2r^2} - \frac{15J_2 a^2 z_e^2}{2r^4}\right) \tag{6.29}$$

$$\ddot{z} = -\frac{z_e \mu}{r^3}\left(1 + \frac{3J_2 a^2}{2r^2} - \frac{15J_2 a^2 z_e^2}{2r^4}\right) \tag{6.30}$$

Equations (6.28), (6.29) and (6.30) are the components of $\ddot{\vec{r}} = (\ddot{x}, \ddot{y}, \ddot{z})$ in the ECEF-frame, given as a function of the position vector $\vec{r} = (x, y, z)$. These are implemented in MATLAB Simulink, for the simulations in chapter 10, by the use of rotation matrices to change between the different reference frames, see chapter 3 and chapter 4.

6.2 Atmospheric Drag

Atmospheric drag acts in the opposite direction of the velocity vector and removes energy from the orbit, causing it to decay. It represents the largest non-gravitational perturbation acting on low altitude satellites (Montenbruck & Gill 2000). Since it is assumed in this thesis that the satellite formation is in an orbit of 600 km altitude, these drag forces can be neglected. For more information on the subject the reader is referred to Pisacane (2000).

6.3 Other Perturbing Forces and Torques

Other perturbing forces that affect the satellites include solar radiation and wind, and other celestial bodies such as the Sun and the Moon. The solar wind is a hot plasma of ions and electrons, while the solar radiation comprises all the electromagnetic waves radiated by the Sun with wavelengths ranging from X-rays to radio waves (Sidi 1997). Since the solar wind is smaller than that of the solar radiation, by a factor of 100 to 1000, it will not be modeled (Grøtli 2005). Perturbing torques are treated in Hughes (1986) and Sidi (1997).

Chapter 7

Hybrid Systems

In this chapter the theory of hybrid systems is introduced. Section 7.2 presents general hybrid system theory, while an overview of the research done on the stability of hybrid systems is given in section 7.3. Several issues and challenges regarding the stability analysis of such a system will be presented. Examples will be given to help clarify some of the theory.

7.1 Introduction

Hybrid systems are dynamical systems with interacting continuous time dynamics and discrete event dynamics (Lygeros, Tomlin & Sastry 2001). They are often represented as a set of states, and a description of how to switch from one state to another. This transition between states might introduce stability issues that make the analysis tools available for non-hybrid systems unapplicable. In general, the analysis and design of hybrid systems is more difficult than that of purely discrete or purely continuous systems, due to the mixed continuous and discrete nature of such a system. The hybrid paradigm has been applied successfully to problems such as automatic control, highway systems, manufacturing and process control (Lygeros, Johansson, Simic, Zhang & Sastry 2003). Lygeros et al. (2001) mention three contexts in which hybrid systems apply:

- **Distributed Control**, the organization of distributed control functions into a *hierarchical architecture*.
- **Multi-modal Control**, which suggests a state-based view, with states representing discrete control modes.
- **Hardware/Software Implementation of a Control Design**, which is ultimately a discrete approximation that interacts through sensors and actuators with a continuous physical environment.

Lately the space industry has adopted the hybrid approach as well, for applications such as spacecraft formation flying and thruster control systems. Spacecraft flying in formation often have several mission objectives to complete. Designing a global control law that satisfies all the requirements for all these objectives during the entire mission could prove to be very difficult. It is therefore attractive to adopt a mode approach instead, with a logic-based switching mechanism to control the transition between the different modes of operation. The thrusters for position control of a satellite can also be modeled as hybrid systems, since they are either on or off, providing discontinuous thrust to the satellite.

7.2 Theory of Hybrid Systems

Theoretical advances and analytical tools are needed to understand the behavior of hybrid dynamical systems. Unfortunately, few techniques for such investigation have been developed. This section introduces some of the theory that has been applied to hybrid systems in the literature. Most of the material is taken from Lygeros (2004) and Lygeros et al. (2001).

A dynamical system describes the evolution of a state over time. Based on the type of their state, dynamical systems can be classified into (Lygeros 2004):

1. **Continuous**, if the state takes values in Euclidean space $\Re^n$ for some n ≥ 1. x $\in \Re^n$ denotes the state of a continuous dynamical system.
2. **Discrete**, if the state takes values in a countable or finite set $\{q_1, q_2, ...\}$. q denotes the state of a discrete system. For example, a light switch is a dynamical system whose state takes on two values, $q \in \{ON, OFF\}$.
3. **Hybrid**, if part of the state takes on values in $\Re^n$ while another part takes values in a finite set. For example, the closed loop system obtained when a computer is used to control an inverted pendulum is hybrid: part of the state (namely the state of the pendulum) is continuous, while another part (the state of the computer) is discrete.

Hybrid dynamical systems can be described by many different modeling languages. One such language, called hybrid automata, is defined below.

7.2.1 Modeling Language: Hybrid Automata

A hybrid automaton is a dynamical system that describes the evolution in time of the values of a set of discrete and continuous state variables (Lygeros et al. 2001).

Definition 7.1 (*Hybrid Automaton*) *A hybrid automaton H is a collection* $H = (Q, X, f, Init, D, E, G, R)$, *where*

- $Q = \{q_1, q_2, ...\}$ *is a finite set of* **discrete states**;
- $X = \Re^n$ *is a finite set of* **continuous states**;
- $f(\cdot, \cdot) : Q \times X \to \Re^n$ *is a* **vector field**;
- $Init \subseteq Q \times X$ *is a set of* **initial states**;
- $Dom(\cdot) : Q \to P(X)$ *is a* **domain**;
- $E \subseteq Q \times Q$ *is a set of* **edges**;
- $G(\cdot) : E \to P(X)$ *is a* **guard condition**;
- $R(\cdot, \cdot) : E \times X \to P(X)$ *is a* **reset map**.

The hybrid automata defined here applies to a class of autonomous hybrid systems with finite continuous and discrete states. An example is given below, found in Lygeros (2004), that shows the use of hybrid automata to model a hybrid system.

Example: Water Tank

The water tank automata, consisting of two tanks containing water, is shown in Figure 7.1.

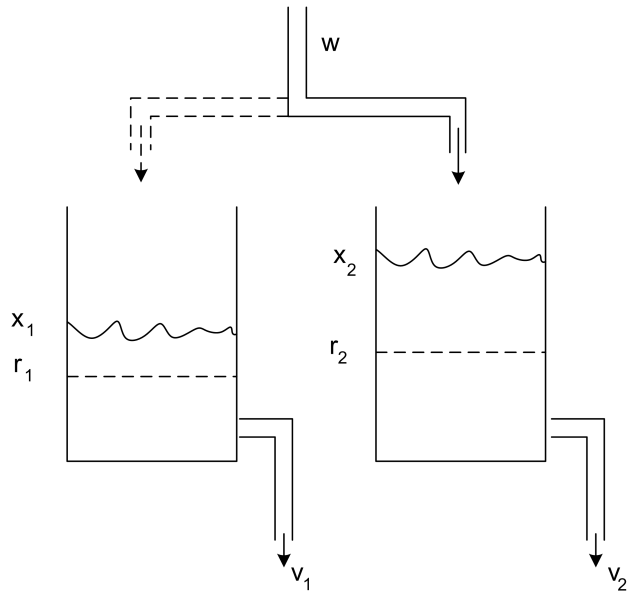

Figure 7.1: Water tank

Let x_i denote the volume of water in tank i. Water flows out of the tanks at a constant rate, $v_i > 0$, with $i = 1, 2$. A hose, dedicated to one tank at a time, adds water to the system at a

constant rate, w. It is assumed that the hose can switch between the tanks instantaneously. The objective is to keep the water volumes above r_1 and r_2, assuming that the initial water volumes are above these initially. To achieve this a controller is used that switches the inflow to tank 1 whenever $x_1 \leq r_1$ and to tank 2 whenever $x_2 \leq r_2$. As in Lygeros (2004), the following hybrid automaton describes this process:

- $Q = \{q_1, q_2\}$;
- $X = \Re^2$;
- $f(q_1, x) = (w - v_1, -v_2)$ and $f(q_2, x) = (-v_1, w - v_2)$;
- $Init = \{q_1, q_2\} \times \{x \in \Re^2 | x_1 \geq r_1 \wedge x_2 \geq r_2\}$;
- $Dom(q_1) = \{x \in \Re^2 | x_2 \geq r_2\}$ and $Dom(q_2) = \{x \in \Re^2 | x_1 \geq r_1\}$;
- $E = \{(q_1, q_2), (q_2, q_1)\}$
- $G(q_1, q_2) = \{x \in \Re^2 | x_2 \leq r_2\}$ and $G(q_2, q_1) = \{x \in \Re^2 | x_1 \leq r_1\}$;
- $R(q_1, q_2, x) = R(q_2, q_1, x) = \{x\}$;

This model is useful when describing other properties of the system, using the stability tools available for hybrid systems. The system is modeled as a directed graph in Figure 7.2.

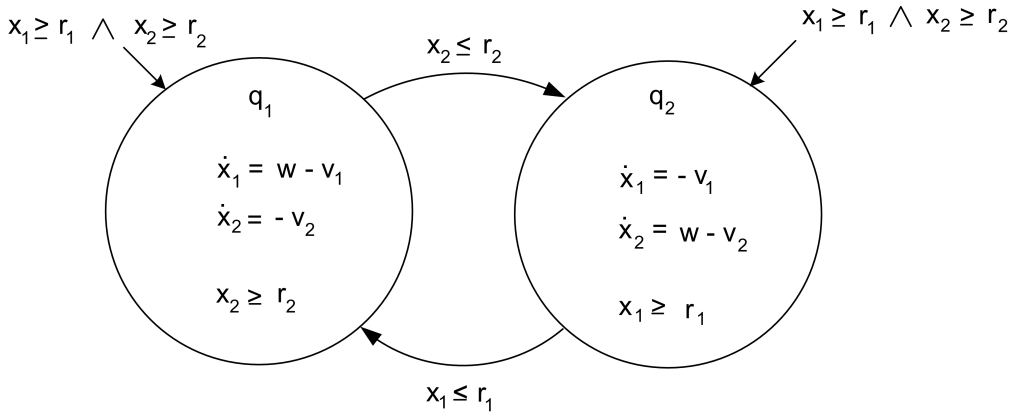

Figure 7.2: Directed graph of the water tank automaton (Lygeros 2004)

7.2.2 Reachability

There has been a growing interest recently in computing reachable sets for various systems (Koo, Pappas & Sastry 2001). Reachability is needed when deriving existence and uniqueness conditions for executions, as well as for several stability results derived for hybrid systems, see Lygeros et al. (2003). Lygeros et al. (2001) states that reachability is also a key concept in the study of safety properties for hybrid systems. When describing a reachable state it is useful to define the concept of a hybrid time trajectory:

Definition 7.2 *(**Hybrid Time Trajectory** (Lygeros et al. 2003)) A hybrid time trajectory is a finite or infinite sequence of intervals* $\tau = \{I_i\}_{i=0}^{N}$, *such that*

- $I_i = \left[\tau_i, \tau_i^{'}\right]$, for all $i < N$;
- if $N < \infty$, then either $I_N = \left[\tau_N, \tau_N^{'}\right]$, or $I_N = \left[\tau_N, \tau_N^{'}\right)$;
- $\tau_i \leq \tau_i^{'} = \tau_{i+1}$ for all i.

where τ_i are the times when discrete transitions take place. Next, we define the concept of execution:

Definition 7.3 *(**Execution** (Lygeros et al. 2003)) An execution of a hybrid automaton H is a collection* $\chi = (\tau, q, x)$, *where* τ *is a hybrid time trajectory,* $q : \langle\tau\rangle \rightarrow \boldsymbol{Q}$ *is a map, and* $x = \{x^i : i \in < \tau >\}$ *is a collection of differentiable maps* $x^i : I_i \rightarrow \boldsymbol{X}$, *such that*

- $(q(0), x^0(0)) \in Init$;
- *for all* $t \in \left[\tau_i, \tau_i^{'}\right)$, $\dot{x}^i(t) = f(q(i), x^i(t))$ and $x^i(t) \in D(q(i))$;
- *for all* $i \in \langle\tau\rangle \ \{N\}$, $e = (q(i), q(i{+}1)) \in E, x^i(\tau_i^{'}) \in G(e)$, and $x^{i+1}(\tau_{i+1}) \in R(e, x^i(\tau_i^{'}))$.

A hybrid automaton H accepts an execution χ if χ satisfies the conditions of Definition 7.3. The concept of reachability can now be defined as (Lygeros 2004):

Definition 7.4 (*Reachable State*) *A state* $(\hat{q}, \hat{x}) \in Q \times X$ *of a hybrid automaton H is called reachable if there exists a finite execution* (τ, q, x) *ending in* $(\hat{q}, \hat{x})$, i.e. $\tau = \left\{[\tau_i, \tau_i^{'}]\right\}_0^N, N < \infty$, *and* $(q_N(\tau_N^{'}), x_N(\tau_N^{'})) = (\hat{q}, \hat{x})$.

Reachability will now be computed for the water tank automaton given as an example in the previous section. The computation is found in Lygeros (2004) and is given here for the sake of completeness and ease of reference.

Example (continued): Water Tank

Assume that $0 < v_1$ and $v_2 < w$. *Reach* must contain all initial states:

$$Reach \supseteq \{q_1, q_2\} \times \left\{x \in \Re^2 | (x_1 \geq r_1) \wedge (x_2 \geq r_2)\right\} \tag{7.1}$$

If

$$(q_i(\tau_i), x_i(\tau_i)) \in Init \tag{7.2}$$

then

$$(q_i(t), x_i(t)) \in Init \tag{7.3}$$

for all $t \in \left[\tau_i, \tau_i^{'}\right]$. Moreover,

$$(q_{i+1}(\tau_{i+1}), x_{i+1}(\tau_{i+1})) \in Init. \tag{7.4}$$

Therefore, by induction on i, $(q_i(t), x_i(t)) \in Init$ for all i and all t, and:

$$Reach \subseteq \{q_1, q_2\} \times \left\{x \in \Re^2 | (x_1 \geq r_1) \wedge (x_2 \geq r_2)\right\} \tag{7.5}$$

Equations (7.1) and (7.5) together imply that:

$$Reach = \{q_1, q_2\} \times \left\{x \in \Re^2 | (x_1 \geq r_1) \wedge (x_2 \geq r_2)\right\} \tag{7.6}$$

7.2.3 Mode Switching

The notion of modes of operation is useful when considering the control of a satellite formation, where each maneuver can be described as a mode or state, with a supervisor controlling the transition between these modes. Typical problems in such a case include formation initialization and deployment, geometrical reconfiguration and other formation flying operations. Mode switching for hybrid systems is an attractive approach compared to its alternative, that is, the design of a global control law for all the subsystems (Mesbahi & Hadaegh 2001). The equation for a typical autonomous switched hybrid system is given below.

A *switched* autonomous system can be described by a differential equation on the form (Branicky 1997):

$$\dot{x} = f_q(x), \quad q \in \{1, ..., N\}, \tag{7.7}$$

where $x \in \Re^n$. Each f_q is assumed to be globally Lipschitz continuous. The value of q at a given time t might depend on just t or the state x, or both. It is also assumed that the q's are picked in such a way that there are finite switches in finite time.

7.3 Stability of Hybrid Systems

Stability of equilibra and invariant sets of hybrid systems has attracted considerable attention. Most of the work in this area has been concentrated on the extension of Lyapunov's direct method, while relatively little work has been done on hybrid versions of other stability analysis tools like LaSalle's invariance theorem and Lyapunov's indirect method. For more information about the extension of the latter two principles, see Hespanha (2004) and Lygeros et al. (2003). Lagrange stability for hybrid dynamical systems is discussed in Ye, Michel & Hou (1998).

Recent extensions of continuous- and discrete-time stability theory to hybrid systems include a study of smooth converse Lyapunov theorems and robust asymptotic stability for hybrid systems (Cai, Teel & Goebel 2005), which in turn enabled the results on input-to-state stability in Cai & Teel (2005). Stability for robust adaptive control of SISO switched linear systems is discussed in El Rifai, El Rifai & Youcef-Toumi (2005).

The following section introduces *multiple Lyapunov functions* as a tool to analyze Lyapunov stability for hybrid systems.

7.3.1 Multiple Lyapunov Functions

A problem that arises when considering the stability of switched systems is that a switched system might become unstable for certain switching signals, even if all the individual subsystems are asymptotically stable. An example of this is given in DeCarlo, Branicky, Pettersson & Lennartson (2000). One approach to prove stability of a switched system is to find a common Lyapunov function for all the systems. Various results on common Lyapunov functions and stability for arbitrary switching are presented in Liberzon & Morse (1999). Another approach is based on the use of multiple Lyapunov functions. This approach is presented below.

The switched autonomous system in (7.7) is used with a switching signal:

$$S = x_0; \quad (q_0, t_0), (q_1, t_1), ..., (q_N, t_N), ... \tag{7.8}$$

where x_0 is the initial state. Assume that the switching sequence is *minimal* in the sense that $q_j \neq q_{j+1}, j \in Z^+$. It is said that V is a candidate Lyapunov function if it is a continuous definite function with continuous partial derivatives. Using the following:

Definition 7.5 (***Lyapunov-Like*** *(Branicky 1997)) Given a strictly increasing sequence of times T in $\Re$, we say that V is a Lyapunov-like function for vector field and trajectory $x(\cdot)$ over T if:*

- $\dot{V}(x(t)) \leq 0$ *for all* $t \in I(T)$,
- *V is monotonically nonincreasing on* $\epsilon(T)$

where the interval completion $I(T)$, of switching times $T = t_0, t_1, ..., t_N$, is the set:

$$\bigcup_{j \in Z^+} (t_{2j}, t_{2j+1}) \tag{7.9}$$

and $\epsilon(T)$ is the *even* sequence of $T : t_0, t_2, t_4, ...$

Theorem 7.1. ***(Multiple Lyapunov Method** (Branicky 1997)**)** Suppose we have candidate Lyapunov functions V_q, $q = 1, ..., N$, and vector fields $\dot{x} = f_q(x)$ with $f_q(0) = 0$ for all q. Let **S** be the set of all switching sequences associated with the system.*

If for each $S \in \boldsymbol{S}$ we have that for all q, V_q is Lyapunov-like for f_q and $x_S(\cdot)$ over $S|q$, then the system is stable in the sense of Lyapunov.

Here $S|q$ denotes the sequence of switching times whose corresponding index is q, and $x_S(\cdot)$ denotes the trajectory described by (7.7) and (7.8). In other words, if V_{q_i} decreases when q_i is active, and V_{q_i} at the time when q_i switched in is less than or equal to V_{q_i} the last time q_i switched in, then the system is Lyapunov stable. The proof of Theorem 7.1, as well as a more detailed explanation of the method, is given in Branicky (1997) and Branicky (1998). Figure 7.3 shows two Lyapunov functions over time. It can be seen from the figure that the value of V_{q_i} is less after switching than the value of V_{q_i} at the last time of switching.

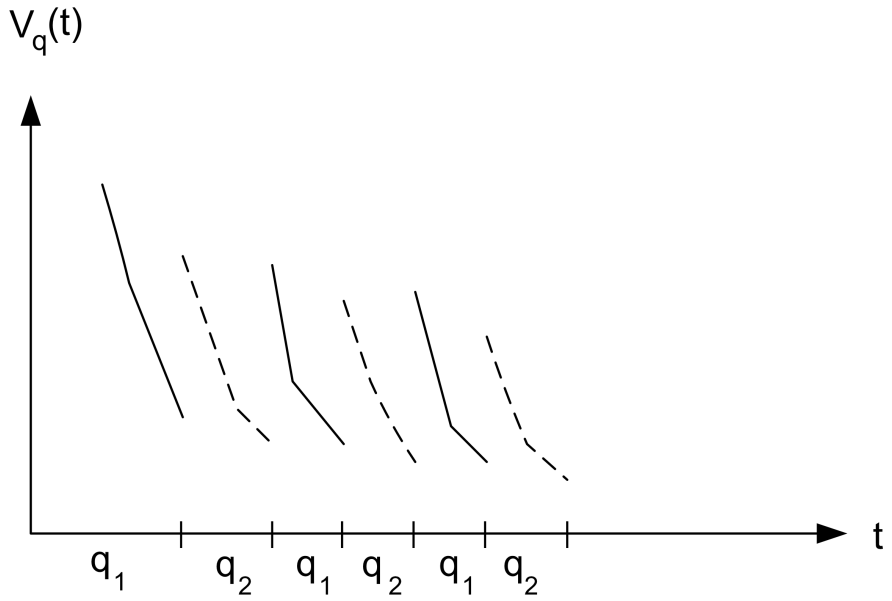

Figure 7.3: Lyapunov function values over time

7.3.2 Slow Switching and Dwell Time

The multiple Lyapunov functions approach deals with systems that switch among vector fields over time or regions of state space (Branicky 1998). This section deals with slow switching and the concept of dwell time, which restricts the class of admissable switching signals and ensures that the interval between two consecutive switching times is no smaller than τ. Under suitable assumptions, a sufficiently large *dwell time* τ guarantees asymptotic stability of the switched system even in the nonlinear case (Liberzon & Morse 1999). The approach below is found in Liberzon & Morse (1999).

Assume for simplicity that all the systems in (7.7) are globally exponentially stable. Then for each $q \in Q$ there exists a Lyapunov function V_q that for some positive constants a_q, b_q and c_q satisfies:

$$a_q|x|^2 \leq V_q(x) \leq b_q|x|^2 \tag{7.10}$$

and

$$\nabla V_q(x) f_q(x) \leq -c_q|x|^2 \tag{7.11}$$

Combinding (7.10) and (7.11) gives:

$$\nabla V_q(x) f_q(x) \leq -\lambda_q V_q(x), \quad q \in Q, \tag{7.12}$$

where $\lambda_q = c_q/b_q$. This implies the following:

$$V_q(x(t_0+\tau)) \leq e^{-\lambda_q \tau} V_q(x(t_0)), \tag{7.13}$$

For simplicity, let's assume that $Q = \{1, 2\}$ and q takes on the value 1 on $[t_0, t_1)$ and 2 on $[t_1, t_2)$, where $t_{i+1} - t_i \geq \tau, i = 0, 1$. Then we have that:

$$V_2(t_1) \leq \frac{b_2}{a_1} V_1(t_1) \leq \frac{b_2}{a_1} e^{-\lambda_1 \tau} V_1(t_0). \tag{7.14}$$

Furthermore:

$$V_1(t_2) \leq \frac{b_1}{a_2} V_2(t_2) \leq \frac{b_1}{a_2} e^{-\lambda_2 \tau} V_2(t_1) \leq \frac{b_1 b_2}{a_1 a_2} e^{-(\lambda_1+\lambda_2)\tau} V_1(t_0). \tag{7.15}$$

It is seen that $V_1(t_2) < V_1(t_0)$ if τ is large enough. An explicit lower bound on τ can be computed so that Theorem 7.1 is satisfied, which means that the system is Lyapunov stable. A general result for the above method is also given in Liberzon & Morse (1999).

7.3.3 Transitioning Nicely Between Modes

Girard (2002) considers the problem of how to switch nicely, from the stability and performance perspectives, between maneuvers. The maneuvers in this case are modes of a supervisory controller. Such a problem can often be reduced to a switching problem between reference trajectories, which is the case of the supervisory control case presented in chapter 9. Transitioning between modes of operation might lead to instability if the difference in desired output is large enough. Two approaches are considered by Girard (2002):

- The safe maneuver approach
- Blending outputs from different trajectory generators

The first approach consists of a safe mode that the system must visit whenever a mode switch occurs. This type of mode is planned to be used in the Proba3[1] mission, where an operation mode is visited between each maneuver once the satellites have finished the formation flying deployment mode, see Figure 7.4.

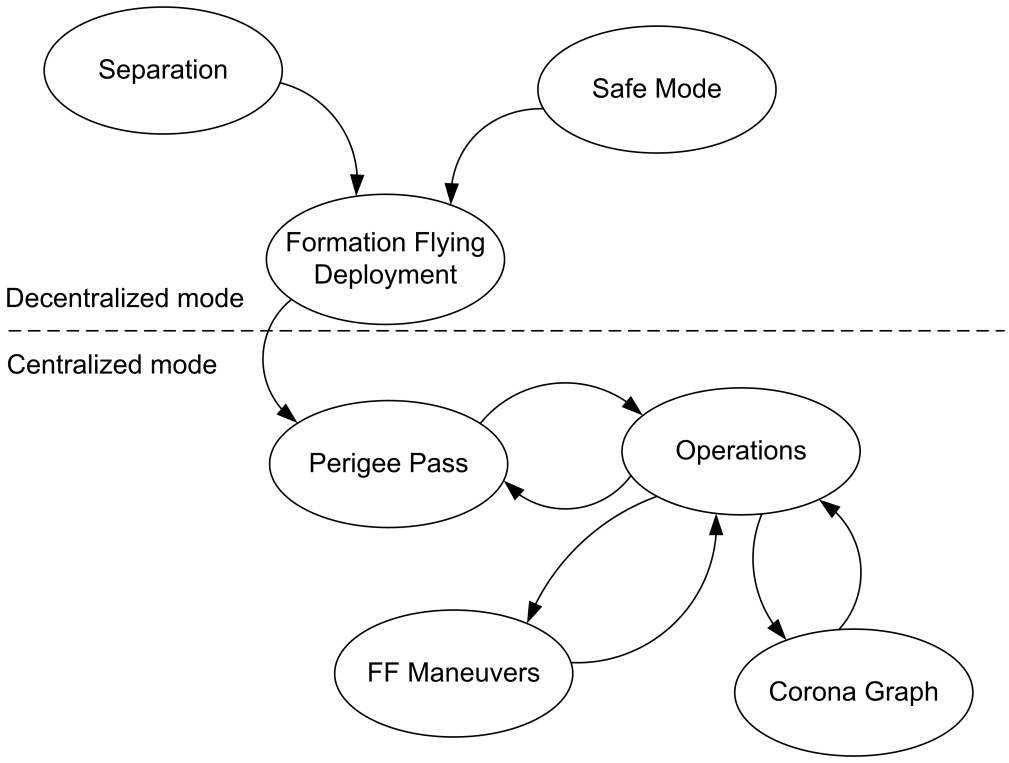

Figure 7.4: Main modes for the Proba3 formation[1]

[1]Information about the Proba3 mission is found in the PROBA3-CDF Study Report: CDF-42(A) (2005). The report also gives explanations of each mode of operation shown in Figure 7.4.

The second approach is to switch smoothly by averaging between the different desired trajectories of the modes. This is similar to using fuzzy-logic like dynamics on the transition (Girard 2002). Figure 7.5 shows the transition between two modes with different desired outputs. The outputs of both maneuver 1 and maneuver 2 are averaged to limit the slope of the switching function.

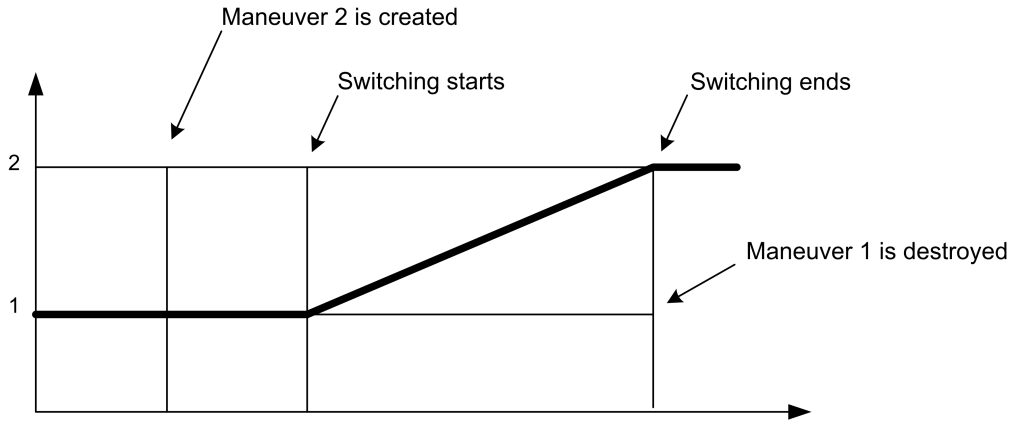

Figure 7.5: Averaging between trajectory generation outputs (Girard 2002)

7.4 Relevant Cases for Position Control of Satellite Formations

For position control of satellite formations the following two cases of hybrid systems are relevant:

- Position control of a spacecraft using thrusters, and
- Supervisory control of a satellite formation

The thruster control case will be discussed in chapter 8, while the latter case will be presented in chapter 9. Simulation results are found in chapter 10.

Chapter 8

Position Control of a Satellite in Formation using Thrusters

The task of the thruster propulsion system is to provide forces and torques that change the translational and angular velocities of the spacecraft. Thruster types are divided into three categories, namely cold gas, electrical and chemical propulsion. In this thesis cold gas thrusters will be used for orbit correction maneuvers of a satellite formation. The thruster control system will be modeled as a switched hybrid system, combining a continuous controller with discrete logic. Hybrid system theory was introduced in chapter 7.

8.1 Propulsion Systems

Thrusters provide force or torque by expelling propellant, such as gas molecules or ions, depending on the type of propulsion used. The amount of thrust can be calculated as follows (Wertz & Larson 1999):

$$\boldsymbol{F} = \frac{dm}{dt}\boldsymbol{V}_e + A_e[P_e - P_\infty] = \frac{dm}{dt}\boldsymbol{V}_e \tag{8.1}$$

where A_e is the nozzle exit area, V_e is the propellant exhaust velocity and $\frac{dm}{dt}$ is the propellant mass flow rate. P_e and P_∞ are the gas and ambient pressures, respectively. Other characteristics that describe the propulsion system include I_{sp} and ΔV. I_{sp} is a measure of the energy content of the propellants, and how efficiently it is converted into thrust, $\boldsymbol{F}$. ΔV is the velocity change that the propulsion can produce, and is the primary measure of system performance capability (Wertz & Larson 1999). General characteristics of several types of propulsion systems are given in Table 8.1.

8.1.1 Cold Gas Thrusters

Cold gas systems are reliable, inexpensive and very low performance systems. They are generally used in applications where simplicity is more important than high performance. The system consists of a controlled, pressurized gas source and a nozzle. The gas is stored under very high pressure, typically $4000 - 10000$ psi (Sidi 1997). This requires tanks capable of withstanding the pressure, resulting in a heavy system. The system has a very low specific impulse, I_{sp}, around 50-75sec is normal. The thrust produced is usually on the order of 5 N.

8.1.2 Electrical Thrusters

Through the use of electrical propulsion the lifetime of the spacecraft or formation can be greatly extended. Electrical propulsion systems have very high specific impulses, ranging from 2000-6000 sec. The disadvantage of using this type of thruster is the low thrust produced, on the order of mN, which is quite small compared to other thruster systems available. Electrical propulsion is divided into 3 types, namely electrothermal, electrostatic and electromagnetic propulsion.

Type	Vacuum I_{sp}(sec)	Thrust Range (N)
Cold Gas	$50 - 75$	$0.05 - 200$
Electrothermal:		
Resistojet	$150 - 700$	$0.005 - 0.5$
Arcjet	$450 - 1500$	$0.05 - 5$
Electrostatic:		
Ion	$2000 - 6000$	$5\text{x}10^{-6} - 0.5$
Colloid	1200	$5\text{x}10^{-6} - 0.05$
Hall Effect	$1500 - 2500$	$5\text{x}10^{-6} - 0.1$
Electromagnetic:		
MPD	2000	$25 - 200$
Pulsed Plasma	1500	$5\text{x}10^{-6} - 0.005$
Pulsed Inductive	4000	$2 - 200$
	2500	$2 - 200$

Table 8.1: General characteristics of propulsion systems (Wertz & Larson 1999)

8.2 Thruster Modeling

When designing a thruster control system it is important to consider both location and direction of the thrusters. This is especially true for attitude control systems, ACS, since the level of torque that the thruster effectively can apply about a satellite axis depends not only

on its thrust level, but also on the torque-arm length about the axis (Sidi 1997).

While attitude thrusters are ideally burned in pairs to produce a pure momentum free torque, position corrections of the orbit are usually accomplished by thrusters acting primarily in the along-track and cross-track directions (Montenbruck & Gill 2000). In the case of orbital maneuvers the overall thruster activity is normally confined to a finite time interval, ranging from seconds or minutes to several hours, depending on the propulsion system. In general six thrusters are needed to allow maneuvers in space, although there are some sophisticated systems that achieve the same result using only four thrusters strategically placed on the satellite body (Sidi 1997).

Since this thesis only treats position control of a Leader/Follower architecture, a simple thruster model will be introduced. For information about thruster arrangement for the attitude case, the reader is referred to Antonsen (2004). A total of 6 thrusters will be used for accurate position control. Two thrusters are placed along each of the three axes of the Hill frame, one in each direction, as shown in Figure 8.1. A precise, functioning attitude system

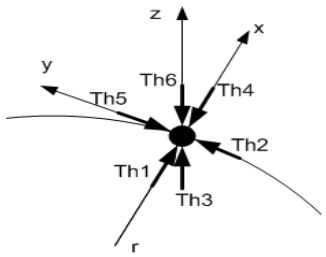

Figure 8.1: Thrusters allocated along the axis of the Hill frame

is assumed, such that the orientation of the reaction thrusters coincide with the respective axes at all times. For simplicity, the center of mass is assumed to coincide with the geometric center of the satellite.

8.3 Thruster Control

In this section several approaches to thruster control will be introduced. Thrusters, unlike other actuators like reaction wheels or control moment gyros, can only provide two types of outputs, on or off. This output is usually a fixed value. To prevent thrusters from firing constantly, causing excessive fuel consumption, several control logics have been designed, such as the bang bang controller and the pulse width pulse frequency (PWPF) modulator. For a more detailed presentation of these two approaches, see for example Wie (1998) and Song & Agrawal (2001).

8.3.1 Bang Bang Controller

The bang bang controller is a simple control scheme that can be used to convert a continuous signal to an on-off type signal suitable for thruster control (Song & Agrawal 2001). In its normal configuration, see Figure 8.2, the bang bang controller fires the thruster when the torque is greater than zero, which may result in excessive fuel consumption.

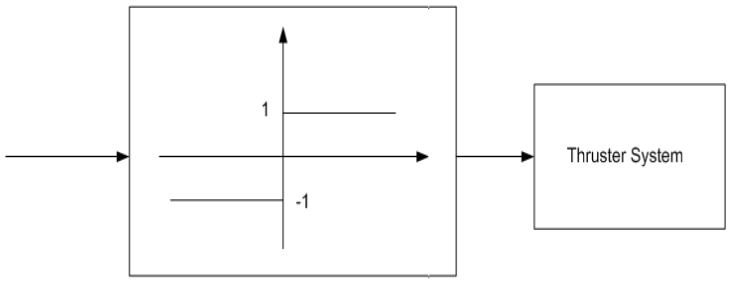

Figure 8.2: Bang bang controller

By using a deadzone, see Figure 8.3, one can reduce the fuel consumption and the number of thruster firings (Song & Agrawal 2001). This variation of the bang bang controller may suffer some reduction in control accuracy, depending on the size of the deadzone. The discontinuous action of the bang bang controller may interact with the flexible modes of the satellite and result in limit cycles (Antonsen 2004)

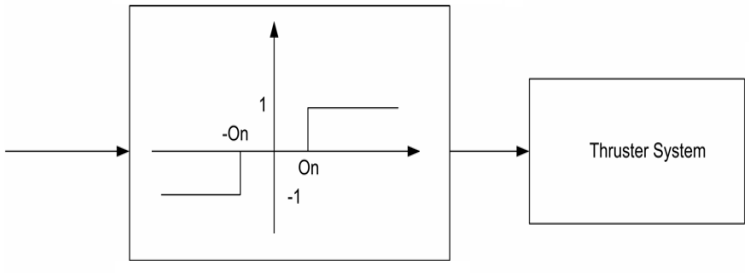

Figure 8.3: Bang bang controller with deadzone

8.3.2 Pulse Width Pulse Frequency Modulator

The pulse width pulse frequency, PWPF, modulator is comprised of a first order filter and a schmitt trigger inside a feedback loop (Wie 1998). A schmitt trigger, see Figure 8.4, is an on-off relay with a deadzone and hysteresis (Topland 2004). The PWPF modulator is shown in Figure 8.5.

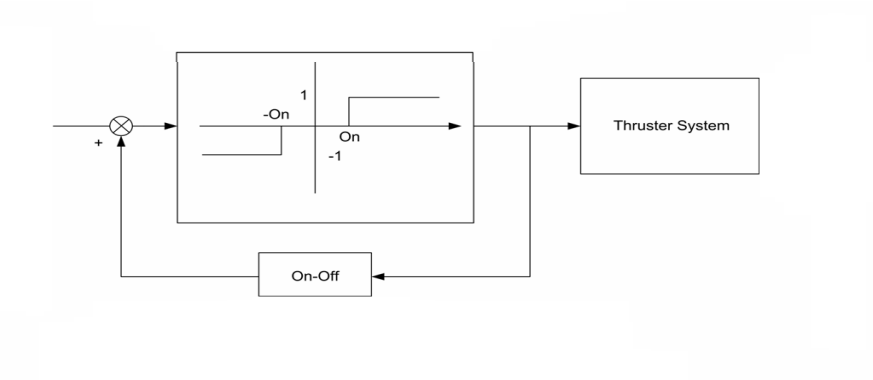

Figure 8.4: Schmitt trigger

The PWPF modulator produces a pulse sequence to the thrusters by adjusting the pulse width and pulse frequency. This scheme has several advantages, such as less vibrations introduced to the spacecraft, improved control accuracy, and reduced fuel consumption, compared to a bang bang controller, with or without a deadzone (Song & Agrawal 2001). On the other hand, the PWPF modulator has many parameters that need to be tuned, a total of four, making it harder to implement than a simple bang bang controller. If these parameters are not tuned properly it could result in excessive fuel consumption, large output phase lag, and even instability of the system (Song & Agrawal 2001). If the sampling frequency is set

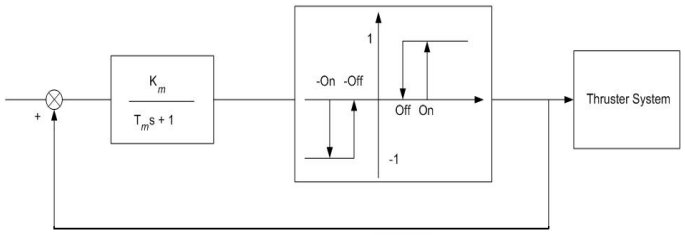

Figure 8.5: Pulse width pulse frequency modulator

to constant, the PWPF modulator reduces to a pulse width modulator. Both approaches are based on the schmitt trigger. For a more detailed analysis of the PWPF modulator the reader is referred to Sidi (1997).

8.4 Thruster Control Case

8.4.1 Design

Thrusters will be used to control the motion of a Follower satellite relative to a Leader satellite in a circular orbit of 600 km altitude around the Earth. The passivity-based controller derived in chapter 9.3 will be used for control. A bang bang controller with a deadzone turns the continuous thrust into on and off control. The thruster control system is modeled as hybrid system, with each set of thrusters, two per axis of the Hill frame, acting as a separate hybrid system. Maximum thrust force is set to 1 N. Figure 8.6 shows the modes of operation for the thruster set in the radial direction, x.

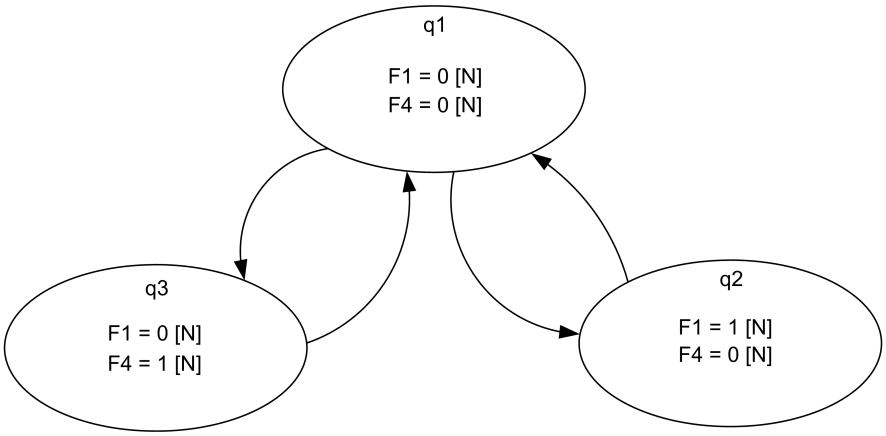

Figure 8.6: Directed graph for the thruster set in the radial direction, F_1 and F_4

Figure 8.6 is explained as follows. The thruster system is in mode q_1 if the Follower satellite is near the desired position, within the set deadzone. If the Follower's relative position drifts from the desired position and outside the deadzone, then the mode will switch to q_2 or q_3, depending on which direction the Follower drifts. The same applies to the other thruster sets, in the y and z directions.

8.4.2 Discussion

One problem with the thruster control system presented in this chapter is the possibility of chattering. Chattering could lead to infinitely fast switching between modes (Liberzon & Morse 1999). One way to prevent this could be to use the concept of *dwell time*, which is discussed in chapter 7.3.2. This is one aspect of the thruster control system that needs to be explored.

Large discontinuities in actuator commands while switching between maneuvers may lead to instabilities (Girard 2002). This problem can be solved by applying the method of smooth switching, which is introduced in chapter 7.3.3. The Stateflow environment in MATLAB

Simulink uses a somewhat similar approach when switching between modes during simulation. This can be seen in chapter 10.1.

Possible future work for the thruster system could be to set up the hybrid system on a form that makes it possible to use the *multiple Lyapunov functions* approach, presented in chapter 7.3.1, to prove Lyapunov stability. As mentioned in chapter 7, stability for all the individual subsystems does not necessarily ensure stability for the entire hybrid system.

Chapter 9

Supervisory Control of a Satellite Formation: Design and Analysis

The formation architecture and modes of operation for the satellite formation, in the supervisory control case, will now be presented. The passivity-based controller that is used in this thesis is also derived, along with an overview of the research done on alternative control schemes. At the end of the chapter the system is analyzed and several design issues are discussed.

9.1 Formation Flying

The concept of formation flying has emerged as an enabling technique that will be used in numerous future satellite missions. Formation flying utilizes many satellites moving in a coordinated fashion to complete missions such as optical interferometry and Earth/Solar observation. Scharf et al. (2004) define formation flying as *a set of more than one spacecraft in which any of the spacecraft dynamic states are coupled through a common control law.*

Distributing the functionality of a large satellite among smaller, less expensive satellites might yield several advantages. The overall weight might be reduced, possibly resulting in lower launch costs. In addition, a spacecraft formation can prove to be more resistant to failures. If, for example, one of the satellites is defect, the operation might not be entirely compromised. By geometrical reconfiguration the satellite formation can continue the mission until it is completed or the flawed satellite has been repaired or replaced. The downside to formation flying is the added complexity for the control and estimation problems (Mesbahi & Hadaegh 1999). According to Mesbahi & Hadaegh (2001), formation flying is among the most relevant applications for adopting a hybrid control approach.

Three approaches to multiagent coordination, such as spacecraft formation flying, robots and aircraft can be found from the literature (Beard, Lawton & Hadaegh 2001):

- Leader/Follower Architecture,
- Behavioral Architecture, and
- Virtual Structure

The Leader/Follower architecture is an hierarchical approach, where one of the agents is designated as the Leader, and the other agents, the Followers, track the position of the Leader with some offset. There are many variants of this approach, including leader tracking, nearest neighbor tracking, barycenter tracking, and other tree topologies (Beard et al. 2001). There is also a leaderless approach, where the Followers track an imaginary Leader satellite, which provides the basic reference motion trajectory for the satellite formation. This approach is used in Yang, Yang, Kapila, Palmer & Vaidyanathan (2002) for fuel optimal control of spacecraft formation reconfiguration, as well as in the thruster control case simulated in chapter 10.1. Yan, Yang, Kapila & de Queiroz (2000) use a Leader/Follower architecture for formation keeping in elliptical orbits around the Earth.

For the Behavioral approach, each spacecraft has several desired behaviors and the control action for each spacecraft is defined by a weighted average of the control for each competing behavior. Formation keeping and collision avoidance are examples of such behaviors.

In the Virtual structure approach, the satellite formation is treated as a single virtual rigid body. The desired states for each satellite in the formation can be specified by the placeholders in the virtual structure. The virtual structure approach has been used in Ren & Beard (2004) for formation feedback control of multiple spacecraft. Lee & Li (2003) propose a similar control scheme, where an average system represents the overall motion of the group and a shape system governs the group formation structure. A coordination architecture that unifies the three approaches mentioned above is introduced in Beard et al. (2001).

The satellite formation in the supervisory control case uses the Leader/Follower architecture, where the Follower satellite track the position of the Leader satellite. In Leader/Follower control, coordination is accomplished through the leading spacecraft. The spacecraft model consists of four satellites S_i. Satellite S_1 is the primary Leader satellite, while satellites S_2, S_3 and S_4 are the Follower satellites. A Supervisor G controls the state transitions of the formation. K_i represents the local controller for the ith satellite. u_i is the control input and y_i is the output from satellite S_i. The architecture is shown in Figure 9.1.

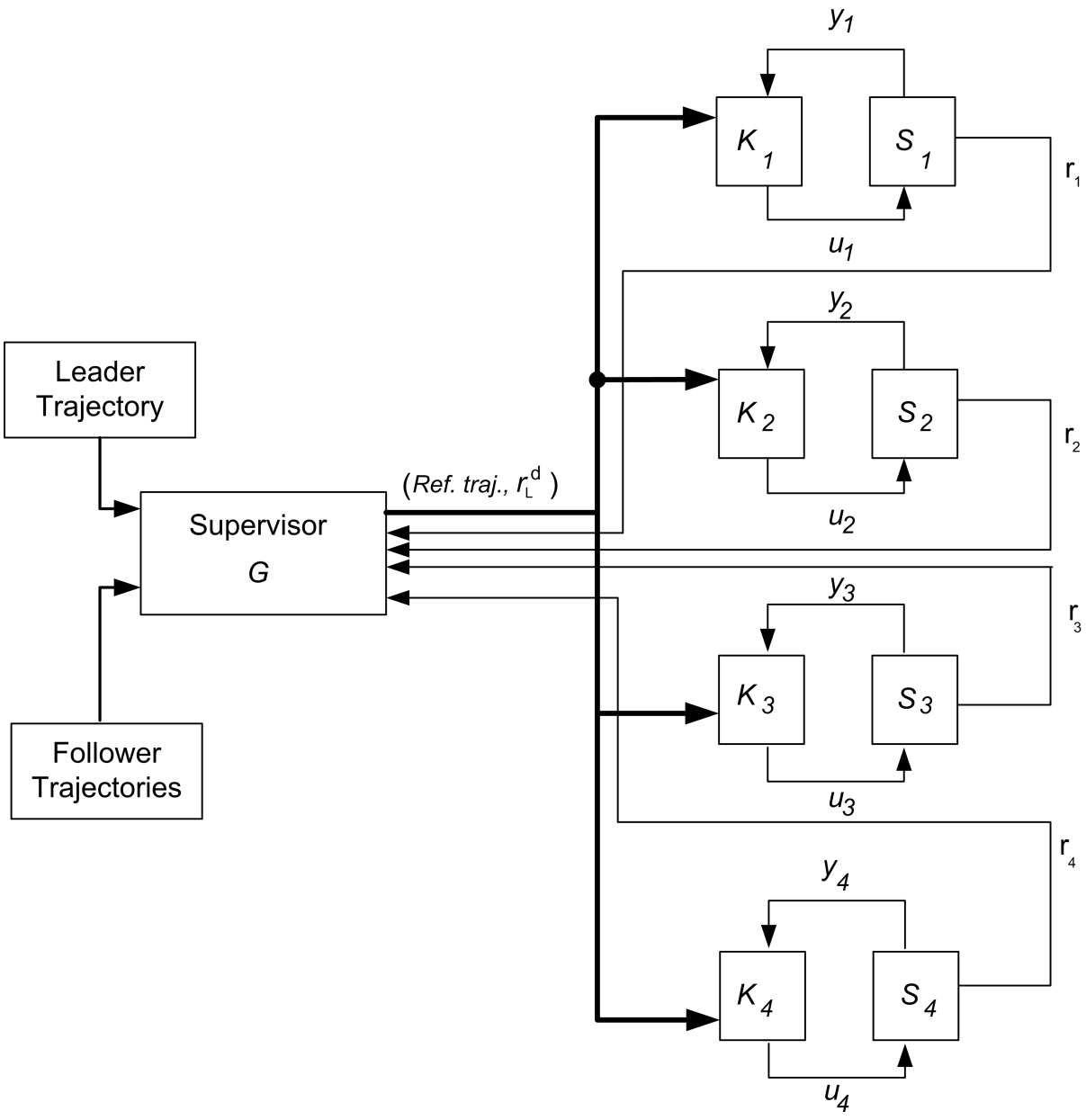

Figure 9.1: Formation flying architecture used in the supervisory control case

9.2 Modes of Operation

A formation of 4 satellites will first be initialized into an along-track (string) formation. The formation will then perform a number of formation flying maneuvers, such as geometrical reconfiguration and leader-reassignment. A supervisor controls the transitions between the different modes. The modes of operation for this satellite formation are shown in Figure 9.2.

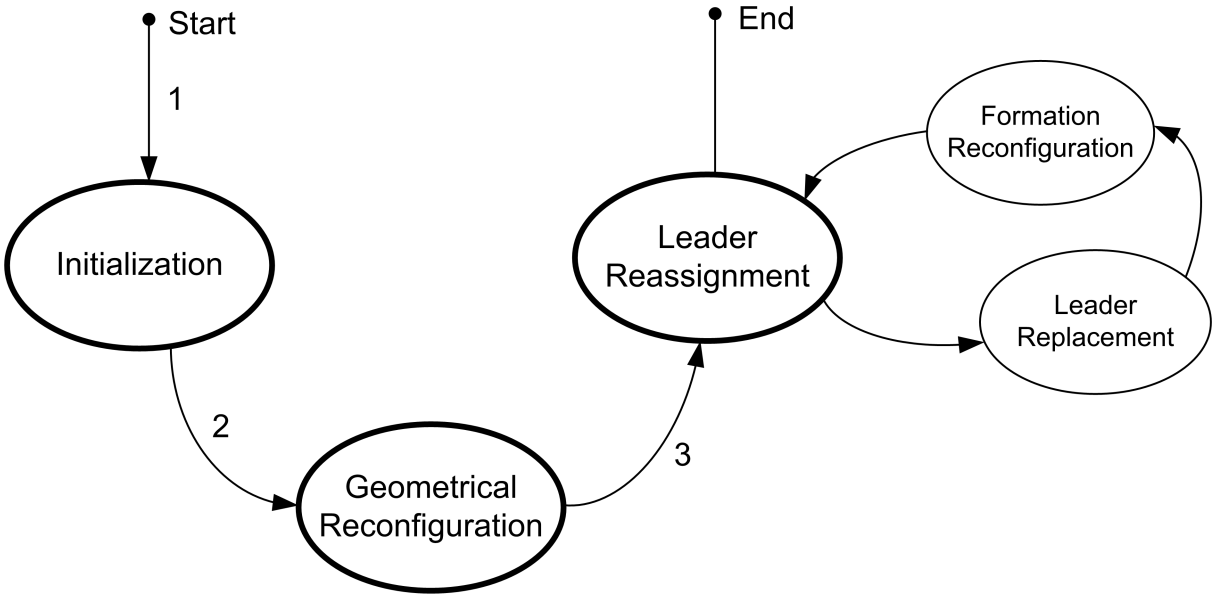

Figure 9.2: Modes of operation

Mode 1 *Initialization* The constellation is initialized into a desired formation pattern, in this case an along-track formation.

Mode 2 *Geometrical Reconfiguration* A geometrical reconfiguration of the formation pattern is performed in this state.

Mode 3 *Leader-Reassignment* Assign a new Leader satellite. This mode is needed if the Leader satellite is malfunctioning.

In mode 1, during the first 200 seconds of operation, the satellite formation is initialized into the desired formation. All the satellites are assumed to start at the same initial position, (0,0,0) in the Hill frame fixed to the Leader satellite S_1, and the Follower satellites are then controlled relative to the Leader satellite such that the desired configuration is reached.

In mode 2, from 200 to 400 seconds, the satellite formation is reconfigured from the along-track formation to a different pattern. Geometrical formation reconfiguration is the process that allows science data acquisition by aligning each spacecraft in a desired configuration. Examples of such configurations include a square projection and an equilateral triangle, used

in Earth/Solar observation and optical interferometry missions, see for example Yang et al. (2002) and Mesbahi & Hadaegh (2001). In this mode the satellite formation takes the first form, a square projection on the Earth.

In the leader-reassignment mode the Leader satellite is replaced by one of the other satellites in the formation, in this case satellite S_4. The formation, now consisting of only three satellites, is then reconfigured into an equilateral triangle. An example of Leader-reassignment is given in Kang, Sparks & Banda (2000), where a control scheme called the perceptive frame is adopted and a rule-based hybrid controller is used to perform formation reconfigurations such as replacing a leader satellite.

9.3 Controllers

Spacecraft formation flying has become an exciting area of research. The concept of distributing the functionality of large spacecraft among smaller, less expensive, cooperative spacecraft is being considered for numerous space missions (Kapila, Sparks, Buffington & Yan 1999). Such a formation relies on control of relative position and orientation between the participating satellites.

In this thesis a passivity-based controller will be used to control the Leader and the Follower satellites in both the thruster control case and the supervisory control case mentioned in chapter 7.4.

9.3.1 Passivity-Based Control

The nonlinear dynamic equations for an m-link robot take the form (Khalil 2000):

$$\boldsymbol{M}(\boldsymbol{q})\ddot{\boldsymbol{q}} + \boldsymbol{C}(\boldsymbol{q}, \dot{\boldsymbol{q}})\dot{\boldsymbol{q}} + \boldsymbol{D}\dot{\boldsymbol{q}} + g(\boldsymbol{q}) = \boldsymbol{u} \tag{9.1}$$

It can be seen that equation (5.30) is quite similar to equation (9.1). This similarity can be used to take advantage of known results for control of robot manipulators when designing a controller for a satellite in formation. Passivity results for a robot manipulator is given in Berghuis & Nijmeijer (1993) and Khalil (2000). A similar controller for a satellite in formation was attained by Grøtli (2005). The latter passivity-based controller will be used in this assignment, and is therefore presented below.

The nonlinear position dynamics are given as (6.28):

$$\mathbf{M}\ddot{\boldsymbol{\rho}} + \boldsymbol{C}(\dot{\nu}, m_f)\dot{\boldsymbol{\rho}} + \mathbf{n}(\boldsymbol{\rho}, \dot{\nu}, \ddot{\nu}, r_l) + \frac{m_f}{m_l}\boldsymbol{u}_l + \boldsymbol{F}_d = \boldsymbol{u}_f$$

The disturbance forces, $\boldsymbol{F}_d$, are not taken into account, and neither are the control forces from the Leader satellite, $\boldsymbol{u}_l$, as they are assumed to be unknown to the Follower satellite(s). Let $\boldsymbol{e} \equiv \boldsymbol{\rho} - \boldsymbol{\rho_d}$ represent the position error. The matrix $\mathbf{C}$ has the property that $\dot{\boldsymbol{M}} - 2\boldsymbol{C}$

is a skew-symmetric matrix and the matrix $\mathbf{M}$ is assumed to be constant. Let the control law be (Grøtli 2005):

$$\boldsymbol{u}_f = \boldsymbol{M}\ddot{\boldsymbol{\rho}}_r + \boldsymbol{C}\dot{\boldsymbol{\rho}}_r + \boldsymbol{n} - \boldsymbol{K}_p\boldsymbol{e} + \boldsymbol{v} \tag{9.2a}$$

$$\boldsymbol{v} = -\boldsymbol{K}_d\boldsymbol{s} \tag{9.2b}$$

where

$$\dot{\boldsymbol{\rho}}_r \equiv \dot{\boldsymbol{\rho}}_d - \boldsymbol{\Lambda}\boldsymbol{e} \tag{9.3}$$

$$\boldsymbol{s} \equiv \dot{\boldsymbol{\rho}} - \dot{\boldsymbol{\rho}}_r = \dot{\boldsymbol{e}} + \boldsymbol{\Lambda}\boldsymbol{e} \tag{9.4}$$

and $\boldsymbol{\Lambda}$, $\boldsymbol{K}_d$, and $\boldsymbol{K}_p$ are symmetric, positive definite matrices. $\mathbf{s}$ is a sliding variable. The Lyapunov stability analysis derived in Grøtli (2005) is presented here for the sake of completeness.

Theorem 9.1. *The tracking controller*

$$\begin{aligned}
\boldsymbol{u}_f &= \boldsymbol{M}\ddot{\boldsymbol{\rho}}_r + \boldsymbol{C}\dot{\boldsymbol{\rho}}_r + \boldsymbol{n} - \boldsymbol{K}_p\boldsymbol{e} - \boldsymbol{K}_d\boldsymbol{s} \\
\dot{\boldsymbol{\rho}}_r &\equiv \dot{\boldsymbol{\rho}}_d - \boldsymbol{\Lambda}\boldsymbol{e} \\
\boldsymbol{s} &\equiv \dot{\boldsymbol{\rho}} - \dot{\boldsymbol{\rho}}_r
\end{aligned}$$

with $\boldsymbol{K}_p$, $\boldsymbol{K}_d$ and $\boldsymbol{\Lambda}$ being symmetric, positive definite matrices, is globally exponentially stable.

Proof. As a storage function candidate

$$V = \frac{1}{2}\boldsymbol{s}^T\boldsymbol{M}\boldsymbol{s} + \frac{1}{2}\boldsymbol{e}^T\boldsymbol{K}_p\boldsymbol{e} \tag{9.5}$$

is chosen, which formally defines a Lyapunov function candidate. Besides being positive definite, it is radially unbounded, and its derivative satisfies

$$\begin{aligned}
\dot{V} &= \boldsymbol{s}^T\boldsymbol{M}\dot{\boldsymbol{s}} + \dot{\boldsymbol{e}}^T\boldsymbol{K}_p\boldsymbol{e} \\
&= \boldsymbol{s}^T(-\boldsymbol{C}\boldsymbol{s} - \boldsymbol{K}_p\boldsymbol{e} - \boldsymbol{K}_d\boldsymbol{s}) + \dot{\boldsymbol{e}}^T\boldsymbol{K}_p\boldsymbol{e} \\
&= -\boldsymbol{s}^T\boldsymbol{K}_d\boldsymbol{s} - (\boldsymbol{s} - \dot{\boldsymbol{e}})^T\boldsymbol{K}_p\boldsymbol{e} \\
&= -\boldsymbol{s}^T\boldsymbol{K}_d\boldsymbol{s} - (\dot{\boldsymbol{e}} + \boldsymbol{\Lambda}\boldsymbol{e} - \dot{\boldsymbol{e}})^T\boldsymbol{K}_p\boldsymbol{e} \\
&= -\boldsymbol{s}^T\boldsymbol{K}_d\boldsymbol{s} - \boldsymbol{e}^T\boldsymbol{\Lambda}\boldsymbol{K}_p\boldsymbol{e}
\end{aligned} \tag{9.6}$$

Hence the system is passive with input $\boldsymbol{v} = -\boldsymbol{K}_d\boldsymbol{s}$ and output $\mathbf{s}$, with V as the storage function. From Lyapunov's direct method, the closed-loop system is globally exponentially stable.

9.3.2 Other Control Schemes

Several other control schemes have been proposed in the literature. A pulse-based periodic control scheme is presented in Kapila et al. (1999) and Yan, Kapila & Sparks (2000). Beard & Hadaegh (1999) consider the problem of deriving control laws for rotating a constellation of spacecraft using on/off thrusters such that the thrusters only fire at the boundaries of a constraint sphere, minimizing the number of times the thrusters fire, thus minimizing fuel consumption. Another control scheme based on sliding mode theory is proposed in Yeh, Nelson & Sparks (2000). For more information about the research done on formation flying control the reader is referred to Scharf et al. (2004).

9.4 Discussion

The supervisory control of a satellite formation has been presented in this chapter. The mission objectives have been modeled as modes of operation, and the switching between these modes depends only on the time t. This time between the switches can be compared to the *dwell time* presented in chapter 7.3.2. Due to the unconstrained motion of each Follower satellite relative to each other, it is proposed that a Follower satellite is independent of other Follower satellites in the formation, as long as it is assumed that the satellites do not collide. This means that if stability is proved for each of the individual Followers relative to the Leader satellite, for all the modes of operation, then the entire system is stable.

All the satellites are modeled by the nonlinear relative position dynamics presented in chapter 5.2 and controlled by the passivity-based controller derived in chapter 9.3. They are therefore globally exponentially stable for each of the individual modes, according to Theorem 9.1. If the time t between mode switching is sufficiently large, then according to the *multiple Lyapunov functions* approach and the *dwell time* approach presented in chapter 7.3.2, the system is stable in the sense of Lyapunov. The problem of how to set up the model on a form that allows for such an analysis should be studied further.

The problem of large jumps in output levels at switching times t can be solved by applying one of the smooth transitioning methods proposed by Girard (2002), see chapter 7.3.3. This could be done in a future extension of the model.

9.4.1 Collision Avoidance Schemes

The supervisory control case, on the form presented in this chapter, uses unconstrained control of the Follower satellites relative to the Leader satellite. A collision avoidance scheme is needed to prevent the Followers from colliding into each other. Many such approaches have been presented in the literature, see for example Kim, Mesbahi & Hadaegh (2003) and Junge & Ober-Blöbaum (2005).

9.4.2 Fuel Optimal Maneuvers

Another issue that needs to be looked into for the supervisory control case is the problem of excessive fuel consumption. Due to different desired trajectories there might be a difference in the amount of fuel consumed by each satellite during execution of the mission objectives. Maintaining even amounts of fuel in each satellite is the problem known as fuel equalization. The latter problem is discussed in Cetin, Bikdash & Hadaegh (2006) for multiple satellites in formation, while Yang et al. (2002) address the problem of fuel minimization for spacecraft formation reconfiguration maneuvers, by designing an efficient hybrid optimization algorithm.

Chapter 10

Simulations

In this chapter the two cases of hybrid systems presented in chapter 8 and chapter 9 will be simulated. The simulations are performed in MATLAB Simulink and the Stateflow environment, using ode45 with a maximum step-size of 10 and a relative tolerance of 10^{-3}. A Leader/Following approach has been chosen for coordinated control of the satellite formations, where the Leader is assumed to to be in an ideal, circular orbit around the Earth. The satellite formation is only influenced by the gravitational forces, including the J2-perturbation. In an orbit of 600 km altitude other perturbing forces have little effect on the satellite formation and are therefore neglected in the satellite model. Furthermore, perfect measurement of both position and velocity is assumed. Simulation data is shown in Table 10.1.

Micro-satellite	
Mass	$m = 70kg$
Initial Conditions	$\boldsymbol{\rho}(0) = [0\ 0\ 0]'$
	$\dot{\boldsymbol{\rho}}(0) = [0\ 0\ 0]'$
Orbit	
Altitude	600km
Inclination	0^o
Eccentricity	$e = 0$ (circular)
Formation	
Architecture	Leader/Follower

Table 10.1: Simulation data

10.1 Position Control of a Satellite in Formation using Thrusters

The relative motion of a Follower satellite relative to a Leader satellite will now be simulated. The continuous passivity-based controller derived in chapter 9.3 will be used for position control. A bang bang controller with a deadzone turns the continuous control into the on-off switched control of a thruster propulsion system. The thrusters are allocated as shown in chapter 8.2. For simplicity the thruster forces are assumed to work in the directions of the Hill frame, meaning that the satellites have functioning attitude control systems.

Parameter	Value
F_{max}	1 N
Deadzone	-0.1 to 0.1
$\mathbf{\Lambda}$	$\begin{bmatrix} 0.9 & 0 & 0 \\ 0 & 0.9 & 0 \\ 0 & 0 & 0.9 \end{bmatrix}$
$\mathbf{K}_p$	$\begin{bmatrix} 4.3 & 0 & 0 \\ 0 & 4.3 & 0 \\ 0 & 0 & 4.3 \end{bmatrix}$
$\mathbf{K}_d$	$\begin{bmatrix} 0.6 & 0 & 0 \\ 0 & 0.6 & 0 \\ 0 & 0 & 0.6 \end{bmatrix}$

Table 10.2: Parameters for thruster control system

Table 10.2 shows the parameters for the thruster control system. The simulation starts with the Leader- and Follower satellite at the same initial position. The satellites travel in an along-track formation in the same circular orbit at 600km altitude, but with the Follower satellite 10 meters behind the Leader satellite. Cold gas propulsion is used with a maximum thrust force of 1 N, where as the deadzone of the bang bang controller is set from -0.1 to 0.1. The results for a thruster position control system using cold gas propulsion is shown in Figure 10.1(a)-(c) and Figure 10.2(a)-(b). It can be seen that the satellites reach the desired formation after approximately 55 seconds, see Figure 10.1(a)-(b). Figure 10.2(a) and 10.2(b) show the forces needed to control the Follower satellite. There is a much higher thruster activity in the radial direction due to the strength of the J_2-perturbation in this direction, which needs to be compensated for. In Figure 10.1(c) the position of the Follower satellite relative to the Leader satellite is plotted, with the Leader satellite at position (x,y,z) = (0,0,0) of the Hill frame. The position of the Follower satellite oscillates slightly near the desired position due to the deadzone implemented in the bang bang controller.

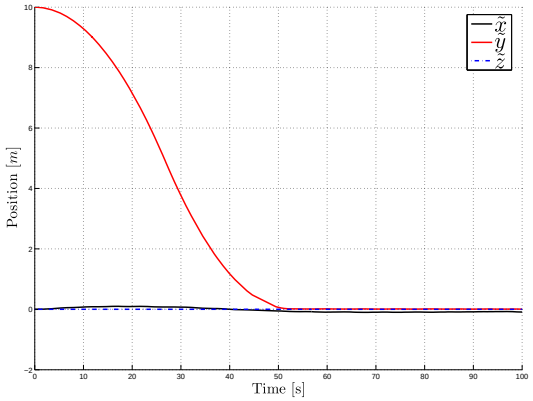

(a) Position error for follower satellite, bang bang control with $F_{max} = 1N$, deadzone =0.1

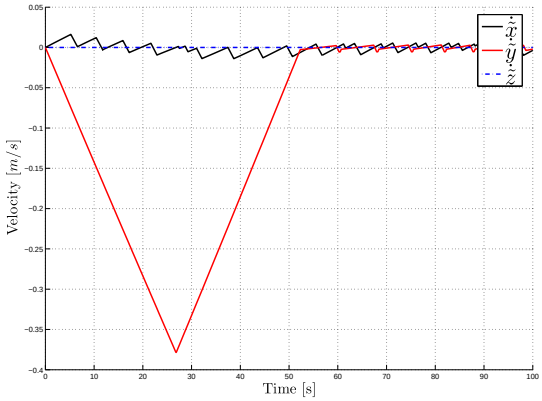

(b) Velocity error for follower satellite, bang bang control with $F_{max} = 1N$, deadzone = 0.1

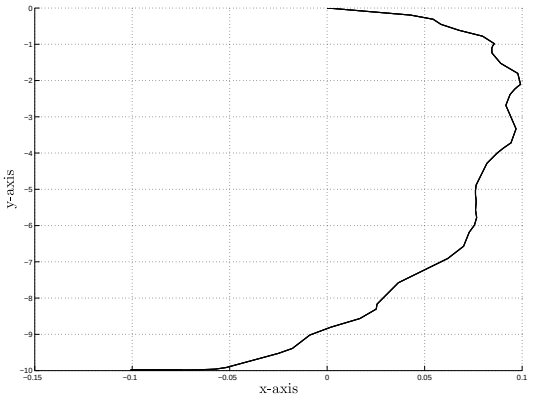

(c) xy-plot of followersatellite, bang bang control with $F_{max} = 1N$, deadzone =0.1

Figure 10.1: Simulation of thruster control system with $F_{max} = 1N$ and deadzone = 0.1, tracking errors

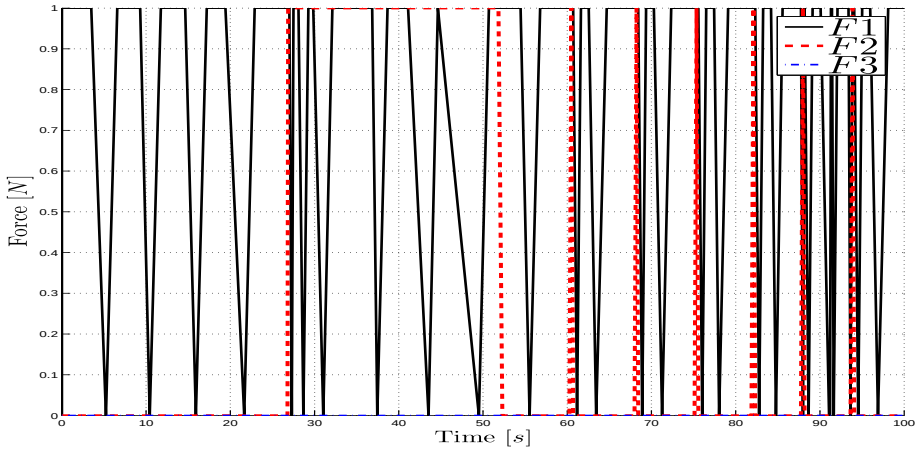

(a) Forces during orbit, bang bang control with $F_{max} = 1N$ and deadzone = 0.1

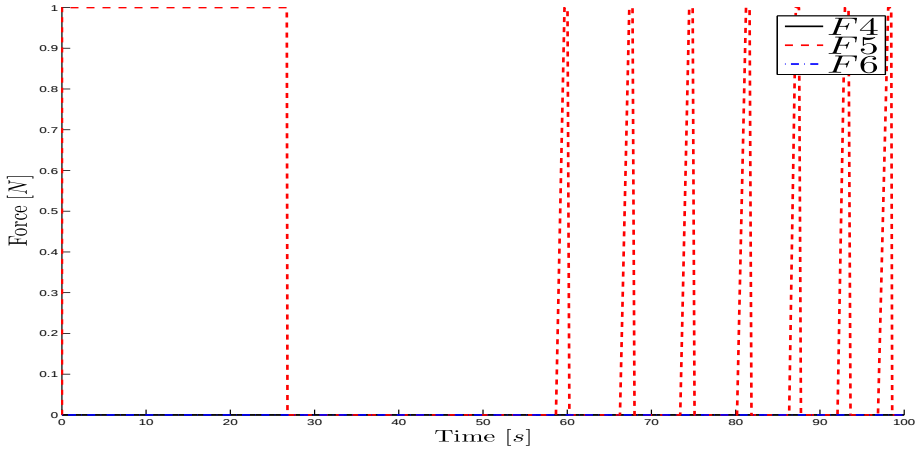

(b) Forces during orbit, bang bang control with $F_{max} = 1N$ and deadzone = 0.1

Figure 10.2: Simulation of thruster control system with $F_{max} = 1N$ and deadzone = 0.1, thruster forces

10.2 Supervisory Control of a Satellite Formation

In this section the modes of the satellite formation described in chapter 9 will be simulated. All the satellites in the formation are influenced by the gravitational forces, including the J_2-effect. As in the previous section, with an altitude of 600 km, other perturbing forces can be neglected. The reference orbit of the Leader satellite has been derived using the Hill-Clohessy-Wiltshire equations. Each satellite uses the proposed continuous passivity-based controller from section 9.3. For more information about the formation flying architecture and the modes of operation used in this simulation, see Figure 9.1 and Figure 9.2. The satellites travel in an along-track formation, with the Follower satellites tracking the position of the Leader satellite. Initial conditions and satellite data are the same as in the previous section, see Table 10.1.

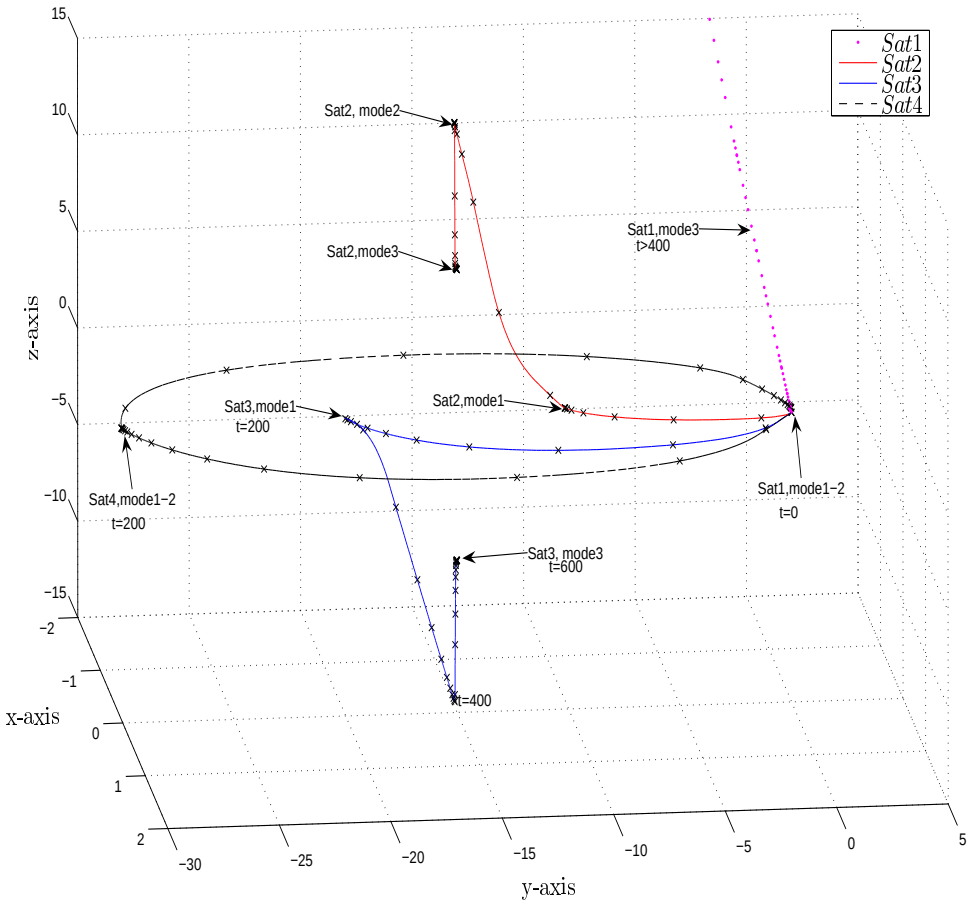

Figure 10.3: 3D plot of the follower satellites' position relative to the leader satellite through the entire operation

Figure 10.3 is a 3D plot that shows the position of each satellite in the formation throughout the simulation. The coordinate system, called the Hill frame, is fixed to the Leader satellite. Simulation is performed for 1000 seconds. Snapshots are taken every 20 seconds, and each cross represents the position of a satellite at time $t_{i+1} = t_i + 20$ seconds, with $t_0 = 0$ and i = 0,2,..,n.

During the first 200 seconds, the satellite formation travels in an along-track formation, with the Follower satellites tracking the position of the Leader satellite. The positions of the Follower satellites are regulated to (0,-10,0) for satellite S_2, (0,-20,0) for satellite S_3, and (0,-30,0) for satellite S_4.

From 200 to 400 seconds, the satellite formation is reconfigured to form a square projection on the yz-plane. The position of satellite S_2 is regulated to (0,-15,15), while the desired position of satellite S_3 is changed to (0,-15,-15). The relative position of satellite S_4 remains the same as in mode 1.

In mode 3, from 400 to 1000 seconds, a Leader-reassignment is performed for the satellite formation. The previous Leader, satellite S_1, is assumed to be malfunctioning, with a disabled control system. Satellite S_1 drifts towards the Earth due to the J_2-perturbation. First, from 400 to 600 seconds, the satellites S_2, S_3 and S_4 are regulated such that they maintain a desired position relative to the reference trajectory developed for the previous Leader satellite, instead of following satellite S_1. Satellite S_4 is controlled such that it replaces satellite S_1 as the Leader satellite. Then, at time t > 600 seconds, the Follower satellites' motion is controlled relative to the new Leader satellite S_4. Now the satellite formation pattern forms an equilateral triangle, with sides of length 15 meters, projected on the yz-plane.

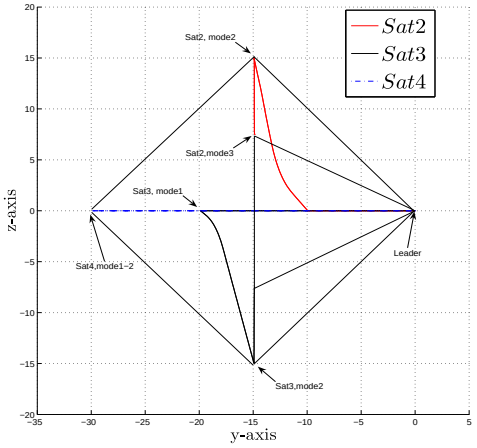

Figure 10.4: Formation patterns of the satellite formation in the yz-plane

The desired formation patterns for the formation flying maneuvers are shown in Figure 10.4. The satellite formation will hold this configuration as the first priority. If the Leader satellite drifts from it's desired reference orbit, due to for example perturbations or slow controller dynamics, the Follower satellites will follow, maintaining the desired relative position and keeping the formation pattern. Table 10.3 shows the parameters for satellite S_1, the primary Leader of the satellite formation.

Parameter	Value
F_{max}	1 N
$\mathbf{\Lambda}$	$\begin{bmatrix} 1.0 & 0 & 0 \\ 0 & 1.0 & 0 \\ 0 & 0 & 1.0 \end{bmatrix}$
$\mathbf{K}_p$	$\begin{bmatrix} 1.6 & 0 & 0 \\ 0 & 1.6 & 0 \\ 0 & 0 & 1.6 \end{bmatrix}$
$\mathbf{K}_d$	$\begin{bmatrix} 0.4 & 0 & 0 \\ 0 & 0.4 & 0 \\ 0 & 0 & 0.4 \end{bmatrix}$

Table 10.3: Parameters for satellite S_1, passivity-based control

Figure 10.5(a) and Figure 10.5(b) show the position- and velocity error of the Leader satellite relative to its desired reference orbit. It can be seen that the passivity-based controller constantly compensates for the J_2-perturbations in the radial direction. After 400 seconds the satellite's closed loop control is disabled to simulate the case where the Leader satellite is defect. This is shown in Figure 10.5(c).

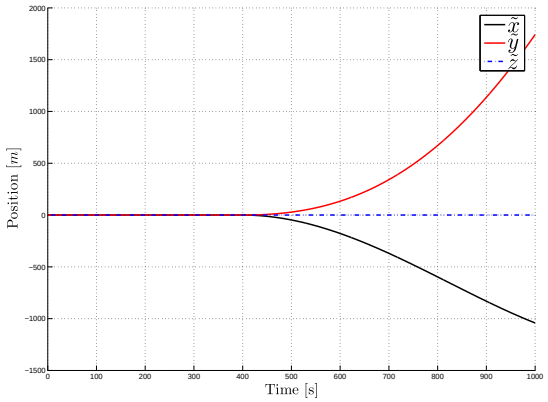

(a) Position error for satellite S_1, passivity-based control with $F_{max} = 1N$

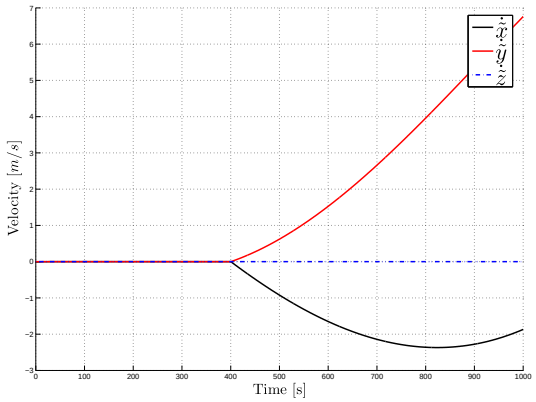

(b) Velocity error for satellite S_1, passivity-based control with $F_{max} = 1N$

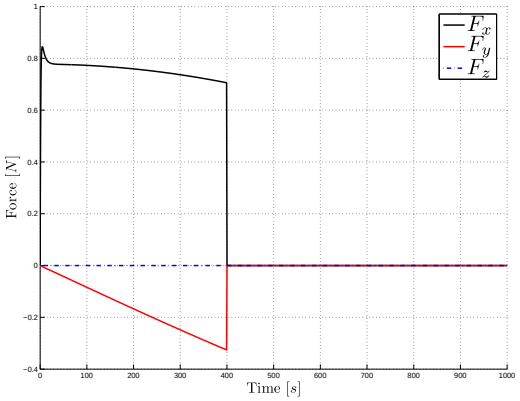

(c) Forces during orbit, passivity-based control with $F_{max} = 1N$

Figure 10.5: Simulation of satellite S_1, $F_{max} = 1N$

Satellites S_2 and S_3 perform the same type of maneuver during the simulated operation, and are therefore modeled with the same parameters for the passivity-based controller, as shown in Table 10.4. The parameters for satellite S_4 are given in Table 10.5. All the parameters have been chosen so that the formation flying maneuvers are completed within reasonable time and with little to no overshoot for the satellites when reaching the desired positions.

Parameter	Value
F_{max}	1 N
$\mathbf{\Lambda}$	$\begin{bmatrix} 1.1 & 0 & 0 \\ 0 & 1.1 & 0 \\ 0 & 0 & 1.1 \end{bmatrix}$
$\mathbf{K}_p$	$\begin{bmatrix} 2.2 & 0 & 0 \\ 0 & 2.2 & 0 \\ 0 & 0 & 2.2 \end{bmatrix}$
$\mathbf{K}_d$	$\begin{bmatrix} 0.4 & 0 & 0 \\ 0 & 0.4 & 0 \\ 0 & 0 & 0.4 \end{bmatrix}$

Table 10.4: Parameters for satellites S_2 and S_3, passivity-based control

Parameter	Value
F_{max}	1 N
$\mathbf{\Lambda}$	$\begin{bmatrix} 1.0 & 0 & 0 \\ 0 & 1.0 & 0 \\ 0 & 0 & 1.0 \end{bmatrix}$
$\mathbf{K}_p$	$\begin{bmatrix} 1.5 & 0 & 0 \\ 0 & 1.5 & 0 \\ 0 & 0 & 1.5 \end{bmatrix}$
$\mathbf{K}_d$	$\begin{bmatrix} 0.4 & 0 & 0 \\ 0 & 0.4 & 0 \\ 0 & 0 & 0.4 \end{bmatrix}$

Table 10.5: Parameters for satellite S_4, passivity-based control

Figure 10.6(a) and 10.6(b) show the position errors and velocity errors, respectively. The desired position and velocity change after 200 seconds and 400 seconds due to mode changes performed by the supervisory controller. It can be seen that the satellite's position- and velocity errors converge to reasonable values after approximately 200 seconds for each mode. A 3D-plot of the motion of the Follower satellite S_2 relative to the Leader S_1 and S_4 throughout the entire operation is given in Figure 10.6(c). Forces needed to perform the formation flying maneuvers are shown in Figure 10.7(a). The same forces are plotted for an extended period of time in Figure 10.7(b). Forces are needed for formation keeping after the formation flying maneuvers as well, to compensate for the J_2-effect.

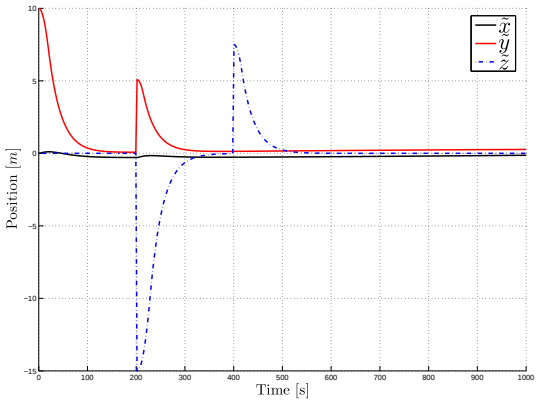

(a) Position error for satellite S_2, passivity-based control with $F_{max} = 1N$

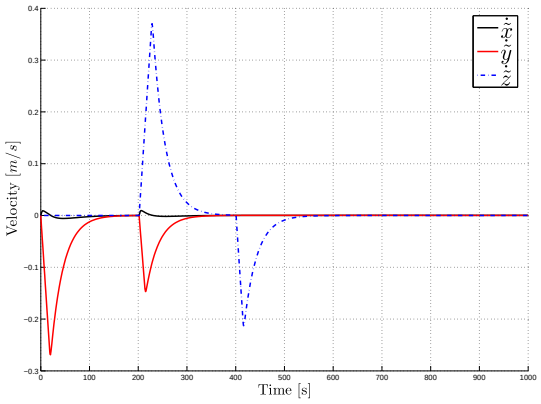

(b) Velocity error for satellite S_2, passivity-based control with $F_{max} = 1N$

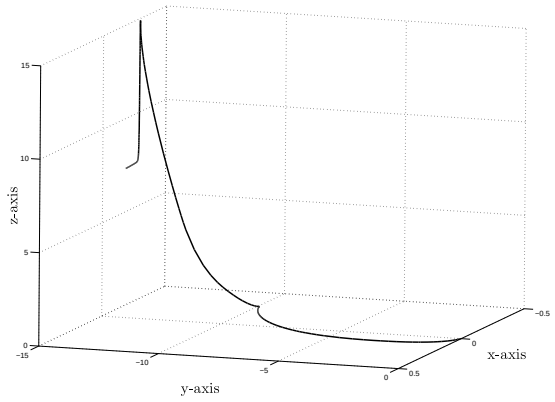

(c) 3D-plot of satellite S_2

Figure 10.6: Simulation of satellite S_2, $F_{max} = 1N$

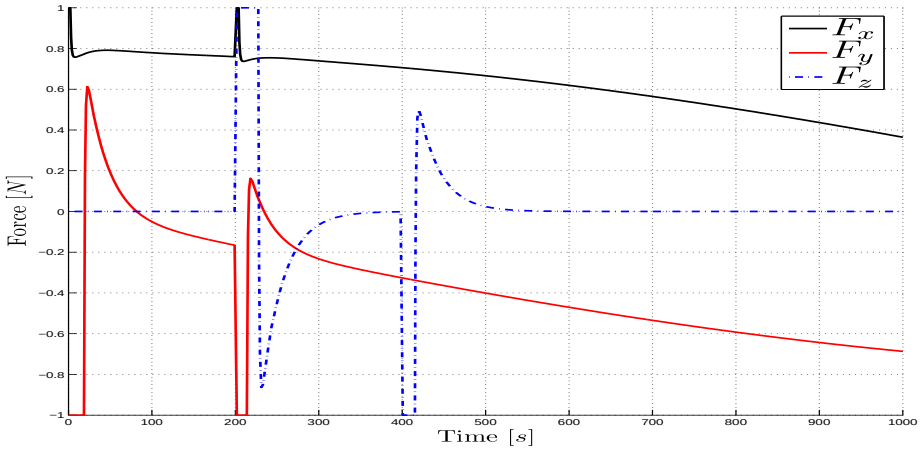

(a) Forces during orbit, passivity-based control with $F_{max} = 1N$

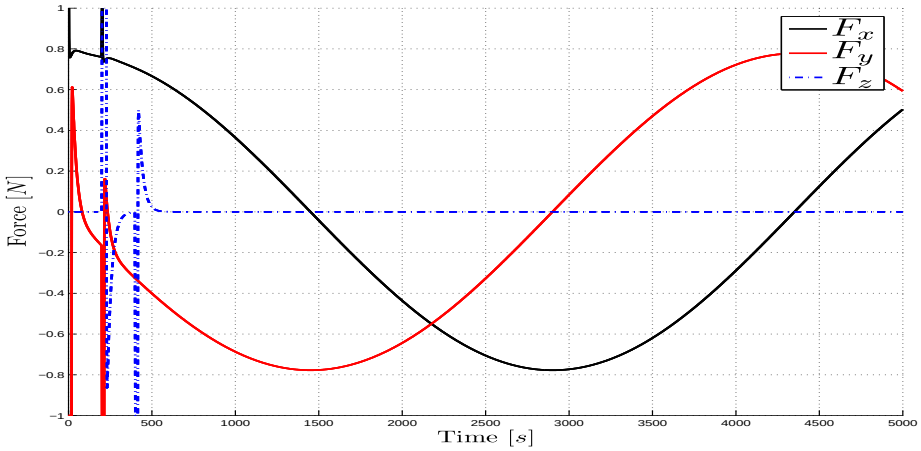

(b) Forces during orbit, passivity-based control with $F_{max} = 1N$

Figure 10.7: Simulation of satellite S_2, $F_{max} = 1N$, forces during orbit

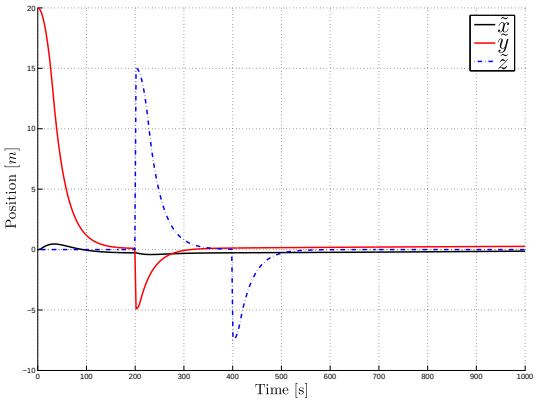

(a) Position error for satellite S_3, passivity-based control with $F_{max} = 1N$

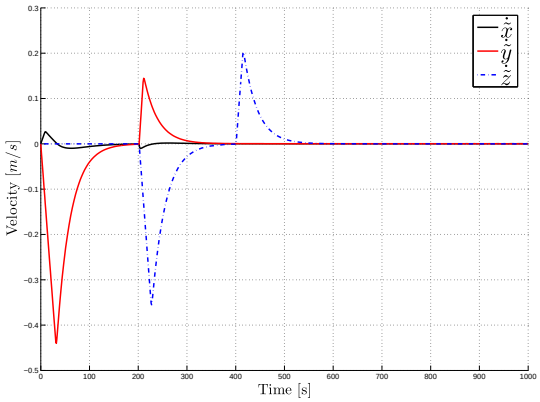

(b) Velocity error for satellite S_3, passivity-based control with $F_{max} = 1N$

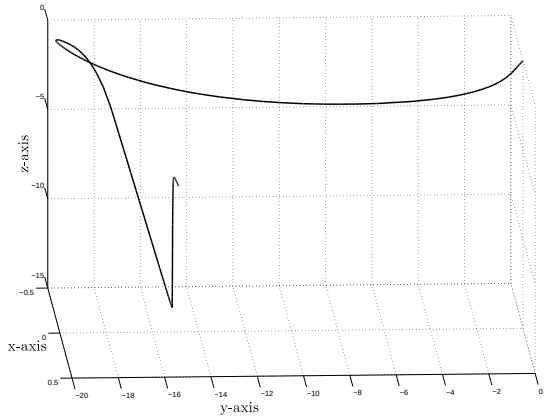

(c) 3D-plot of satellite S_3

Figure 10.8: Simulation of satellite S_3, $F_{max} = 1N$

Figure 10.8(a)-(c) show the simulation results for satellite S_3, which has the same control parameters as satellite S_2, but follows different reference trajectories. Figure 10.8(a) and 10.8(b) show that the position and velocity errors are within reasonable values after approximately 200 seconds for each mode. Figure 10.8(c) is a 3D-plot of the satellite's relative motion, while the thruster forces needed to control the satellite are plotted in Figure 10.9(a), with the same forces plotted for an extended duration in Figure 10.9(b). The parameters for the passivity-based controller are chosen such that the satellite has relatively slow dynamics, with little to no overshoot. Due to the time it takes for satellite S_4 to reach its desired position, faster dynamics are not necessary.

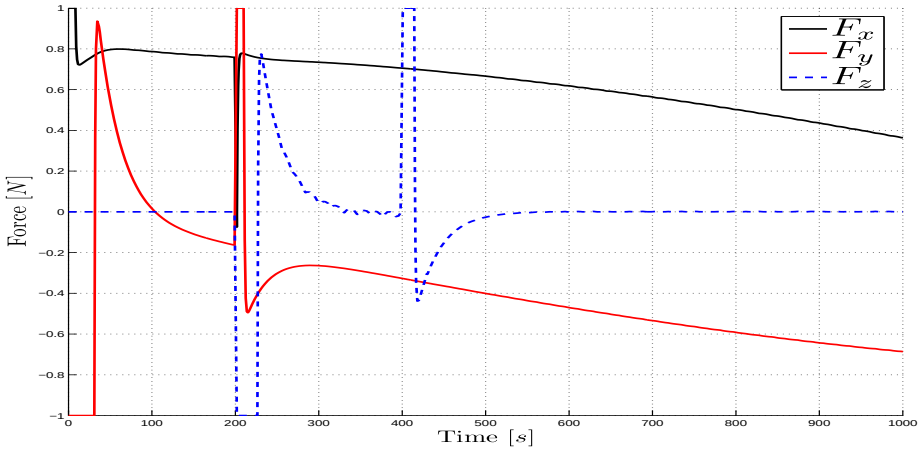

(a) Forces during orbit, passivity-based control with $F_{max} = 1N$

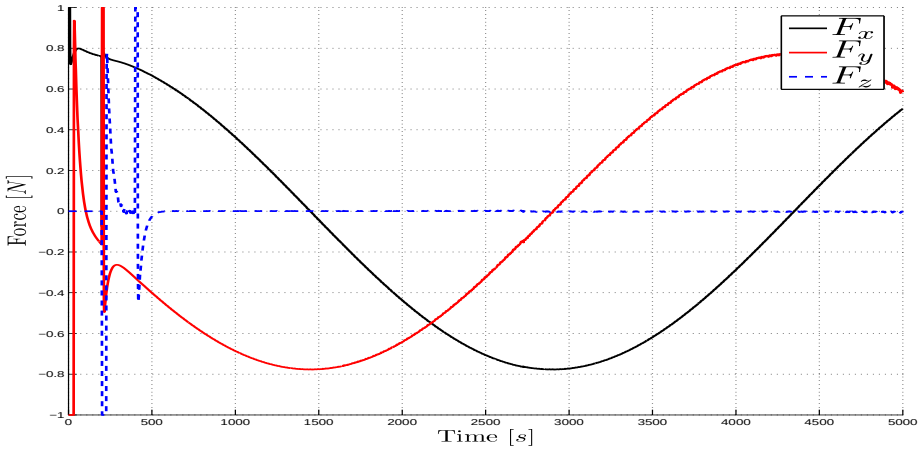

(b) Forces during orbit, passivity-based control with $F_{max} = 1N$

Figure 10.9: Simulation of satellite S_3, $F_{max} = 1N$, forces during orbit

In mode 1, the Follower satellite S_4 reaches its desired position relative to the Leader satellite S_1 within 200 seconds, see Figure 10.10(a) and 10.10(b). In the Leader reassignment mode, satellite S_4 reaches its desired orbit after approximately 200 seconds, where it follows the Leader reference trajectory for the rest of the operation, with satellites S_2 and S_3 as its Follower satellites. The input forces needed to control the satellite are plotted in Figure 10.11(a)-(b), where as a 3D model depicts the satellite's motion in Figure 10.10(c).

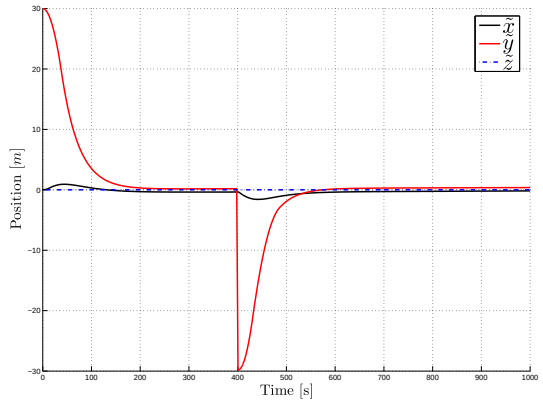

(a) Position error for satellite S_4, passivity-based control with $F_{max} = 1N$

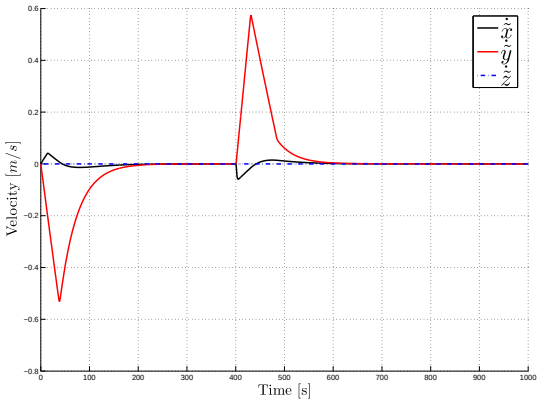

(b) Velocity error for satellite S_4, passivity-based control with $F_{max} = 1N$

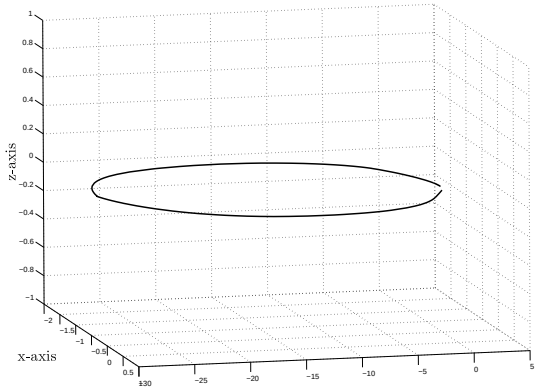

(c) 3D-plot of satellite S_4

Figure 10.10: Simulation of satellite S_4, $F_{max} = 1N$

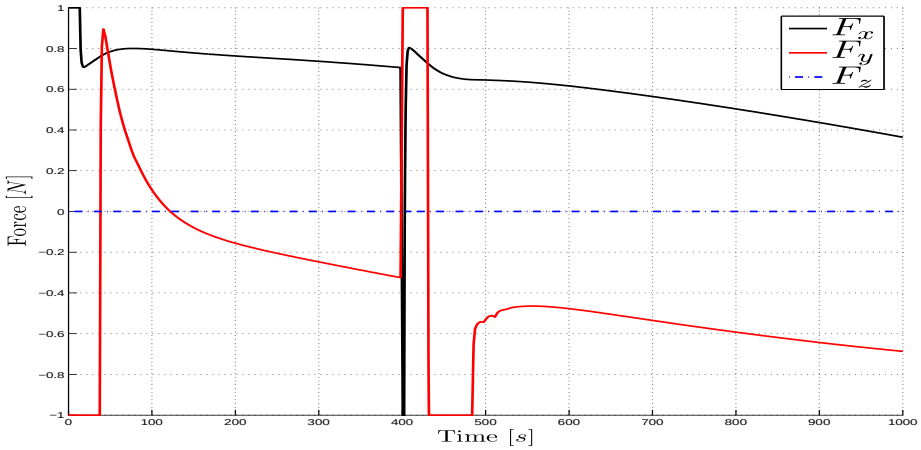

(a) Forces during orbit, passivity-based control with $F_{max} = 1N$

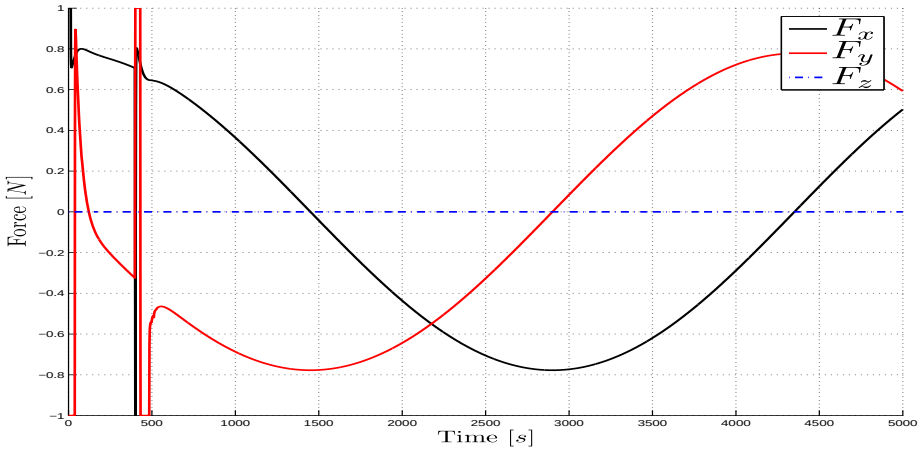

(b) Forces during orbit, passivity-based control with $F_{max} = 1N$

Figure 10.11: Simulation of satellite S_4, $F_{max} = 1N$, forces during orbit

Chapter 11

Concluding Remarks and Recommendations

11.1 Conclusion

In this thesis a linear model for the relative position dynamics of a Leader/Follower spacecraft formation, called the Hill-Clohessy-Wiltshire equations, has been presented. The linear model was then extended to a nonlinear version, which has been used to model the satellite formations. A passivity-based controller was used for each satellite, to perform formation flying maneuvers and to compensate for perturbations, such as the J_2-effect. The Hill-Clohessy-Wiltshire equations have been used to derive fuel efficient paths for the satellite formations orbiting the Earth.

The theory of hybrid systems has been introduced, as well as an overview of the research done on stability theory for hybrid systems. Two relevant cases for hybrid control of satellite formations have been investigated, namely the thruster control case and the supervisory control of a satellite formation. In the latter case, the concept of modes of operation has been used to switch between different desired maneuvers, such as geometrical reconfiguration and leader-reassignment. Simulations were performed in MATLAB Simulink and the Stateflow environment for the hybrid control of the cases mentioned above.

11.2 Recommendations

The dynamic model used in this thesis is only 3DOF. The model could be extended to include relative attitude dynamics. Furthermore, controllers and observers would need to be designed to control the orientation of the satellites. In addition, a pulse width pulse frequency modulator could be implemented instead of the bang bang controller for the thruster control case. A PWPF modulator provides better accuracy and results in less power consumption

if tuned correctly, but the selection of the modulator parameters poses a challenge (Song & Agrawal 2001).

Perfect measurement of both position and velocity was assumed in this thesis. In Grøtli (2005) a combined controller-observer design was proposed for the continuous case, when it was assumed that only position measurements were available. The same could be tested for the discontinuous control scheme used in this dissertation. Robustness properties could be investigated by introducing estimation- and measurement disturbances.

Another future extension to this thesis could be to investigate how to set up the models for both the thruster control case and the supervisory control case on a form that enables us to analyze the system with existing stability theory for hybrid systems. One way to achieve this could be to simulate the satellite formation for the supervisory control case for several orbits around the Earth, and to apply the safe maneuver approach described in and chapter 7.3.3 and Girard (2002). A lot of work remains to be done for the stability analysis of nonlinear hybrid systems. Further investigation of this topic is needed.

Furthermore, the satellite formation for the supervisory control case could be simulated with parameters similar to those proposed for the future Proba3 mission. This includes using eccentric orbits instead of circular orbits, as well as a higher inclination. The study of the modes of operation in such a case would be of interest.

As mentioned in chapter 9.4, a collision avoidance scheme should be incorporated in the model, possibly as a mode of operation. An investigation of the fuel efficiency of the satellite formation control should be performed as well. These topics are discussed thoroughly in the literature.

Appendix A

CD Contents

The included CD contains a PDF version of this report and the MATLAB source files for the two cases that were simulated.

File	Description	Location
AuneMaster.pdf	PDF version of the report	\AuneMaster.pdf
Thruster.mdl	Simulink model of the thruster control case	\Thruster\Thruster.mdl
initThruster.m	Init for the thruster control case.	\Thruster\initThruster.m
plotting.m	Generates plots from the simulation.	\Thruster\plotting.m
Supervisor.mdl	Simulink model of the supervisory control case	\Supervisor\Supervisor.mdl
initSupervisor.m	Init for the supervisory control case.	\Supervisor\initSupervisor.m
plottingSat1.m	Generates plots for satellite 1.	\Supervisor\plottingSat1.m
plottingSat2.m	Generates plots for satellite 2.	\Supervisor\plottingSat2.m
plottingSat3.m	Generates plots for satellite 3.	\Supervisor\plottingSat3.m
plottingSat4.m	Generates plots for satellite 4.	\Supervisor\plottingSat4.m

Table A.1: CD contents

References

Antonsen, J. (2004), Attitude control of a micro satellite with the use of reaction control thrusters, Master's thesis, HiN, Department of Computer Science, Electrical Engineering and Space Technology.

Beard, R. W. & Hadaegh, F. Y., eds (1999), *Finite Thrust Control for Satellite Formation Flying with State Constraints*, Proceedings of the American Control Conference, San Diego, California.

Beard, R. W., Lawton, J. & Hadaegh, F. Y. (2001), 'A coordination architecture for spacecraft formation control', *IEEE Transactions on Control Systems Technology* **Vol. 9, No. 6**.

Berghuis, H. & Nijmeijer, H. (1993), 'A passivity approach to controller-observer design for robots', *IEEE Transactions on Robotics and Automation* **Vol. 9, No. 6**.

Branicky, M. S., ed. (1997), *Stability of Hybrid Systems: State of the Art*, Proceedings of the 36th Conference on Decision & Control, San Diego, California.

Branicky, M. S., ed. (1998), *Multiple Lyapunov Functions and Other Analysis Tools for Switched and Hybrid Systems*, Proceedings of the American Control Conference, San Diego, California.

Cai, C. & Teel, A. R., eds (2005), *Results on Input-to-State Stability for Hybrid Systems*, Proceedings of the 44th IEEE Conference on Decision and Control, and the European Control Conference, Seville, Spain.

Cai, C., Teel, A. R. & Goebel, R., eds (2005), *Converse Lyapunov Theorems and Robust Asymptotic Stability for Hybrid Systems*, Proceedings of the American Control Conference, Portland, OR, USA.

Cetin, B., Bikdash, M. & Hadaegh, F. Y., eds (2006), *Optimal Fuel Equalization for Formation Reconfiguration Using Mixed Integer-Linear Programming*, Proceedings of the 38th Southeastern Symposium on System Theory, Tennessee Technological University, Cookeville, TN, USA.

Clohessy, W. H. & Wiltshire, R. S. (1960), 'Terminal guidance system for satellite rendezvous', *Journal of the Aerospace Sciences* **Vol. 27**.

DeCarlo, R. A., Branicky, M. S., Pettersson, S. & Lennartson, B., eds (2000), *Perspectives and Results on the Stability and Stabilizability of Hybrid Systems*, Vol. Vol. 88, No. 7, Proceedings of the IEEE.

Egeland, O. & Gravdahl, J. T. (2002), *Modeling and Simulation for Automatic Control*, Marine Cybernetics.

El Rifai, K., El Rifai, O. & Youcef-Toumi, K., eds (2005), *On Robust Adaptive Switched Control*, Proceedings of the American Control Conference, Portland, OR, USA.

Fossen, T. I. (2002), *Marine Control Systems*, Tapir Trykk.

Girard, A. R. (2002), Hybrid System Architectures for Coordinated Vehicle Control, PhD thesis, University of California, Berkeley.

Grøtli, E. I. (2005), Modeling and control of formation flying satellites in 6 dof, Master's thesis, NTNU, Department of Engineering Cybernetics.

Hespanha, J. P. (2004), 'Uniform stability of switched linear systems: Extensions of lasalle's invariance principle', *IEEE Transactions on Automatic Control* **Vol. 49, No. 4**.

Hughes, P. C. (1986), *Spacecraft attitude dynamics*, John Wiley & Sons.

Junge, O. & Ober-Blöbaum, S., eds (2005), *Optimal Reconfiguration of Formation Flying Satellites*, Proceedings of the 44th IEEE Conference on Decision and Control, and the European Control Conference, Seville, Spain.

Kang, W., Sparks, A. & Banda, S., eds (2000), *Multi-Satellite Formation and Reconfiguration*, Proceedings of the American Control Conference, Chicago, Illinois.

Kapila, V., Sparks, A. G., Buffington, J. M. & Yan, Q., eds (1999), *Spacecraft Formation Flying: Dynamics and Control*, Proceedings of the American Control Conference, San Diego, California.

Khalil, H. K. (2000), *Nonlinear Systems*, Pearson Education International Inc.

Kim, Y., Mesbahi, M. & Hadaegh, F. Y., eds (2003), *Multiple-Spacecraft Reconfigurations through Collision Avoidance, Bouncing, and Stalemates*, Proceedings of the American Control Conference, Denver, Colorado.

Koo, J. T., Pappas, G. J. & Sastry, S. (2001), 'Mode switching synthesis for reachability specifications'.

Kristiansen, R., Loria, A., Chaillet, A. & Nicklasson, P. J. (2006), 'Output feedback control of a relative translation in a leader-follower spacecraft formation', *in Group Coordination and Cooperative Control* . Pettersen, K. Y. and Gravdahl, J. T. and Nijmeijer, H., eds, Springer-Verlag.

Krogstad, T. (2005), Attitude control of satellites in clusters, Master's thesis, NTNU, Department of Engineering Cybernetics.

Lee, D. & Li, P. Y., eds (2003), *Formation and Maneuver Control of Multiple Spacecraft*, Proceedings of the American Control Conference, Denver, Colorado.

Liberzon, D. & Morse, A. S. (1999), 'Basic problems in stability and design of switched systems', *IEEE Control Systems Magazine* **Vol. 19, No. 5**.

Lygeros, J. (2004), Lecture notes on hybrid systems. [Available online: http://robotics.eecs.berkeley.edu/∼sastry/ee291e/lygeros.pdf], [Last accessed: 01.06.2006].

Lygeros, J., Johansson, K. H., Simic, S. N., Zhang, J. & Sastry, S. S. (2003), 'Dynamical properties of hybrid automata', *IEEE Transactions on Automatic Control* **Vol. 48, No. 1**.

Lygeros, J., Tomlin, C. & Sastry, S. (2001), Art of hybrid systems. [Available online: http://robotics.eecs.berkeley.edu/∼sastry/ee291e/book.pdf], [Last accessed: 01.06.2006].

Mesbahi, M. & Hadaegh, F. Y., eds (1999), *Formation Flying Control of Multiple Spacecraft via Graphs, Matrix Inequalities, and Switching*, Proceedings of the 1999 IEEE, Kohala Coast-Island of Hawai'i, Hawai'i, USA.

Mesbahi, M. & Hadaegh, F. Y., eds (2001), *Mode and Logic-based Switching for the Formation Flying Control of Multiple Spacecraft*, Proceedings of the American Control Conference, Arlington, VA.

Montenbruck, O. & Gill, E. (2000), *Satellite Orbits*, Springer.

Pisacane, V. L. (2000), *Fundamentals of Space Systems, Second Edition*, Springer.

Ren, W. & Beard, R. W., eds (2004), *Formation Feedback Control for Multiple Spacecraft via Virtual Structures*, Vol. Vol. 151, No. 3, IEE Proc.-Control Theory Appl.

Rodriguez-Angeles, A. (2002), Synchronization of Mechanical Systems, PhD thesis, Techniche Universiteit Eindhoven.

Scharf, D., Hadaegh, F. Y. & Ploen, S. R., eds (2003), *A survey of Spacecraft Formation Flying Guidance and Control (Part I): Guidance*, Proceedings of the American Control Conference, Denver, Colorado.

Scharf, D., Hadaegh, F. Y. & Ploen, S. R., eds (2004), *A survey of Spacecraft Formation Flying Guidance and Control (Part II): Control*, Proceedings of the American Control Conference, Boston, Massachusetts.

Schwartz, J. L. (2004), The Distributed Spacecraft Attitude Control System Simulator: From Design Concept to Decentralized Control, PhD thesis, Virginia State University.

Sciavicco, L. & Siciliano, B. (2005), *Modelling and Control of Robot Manipulators*, Springer.

Sidi, M. J. (1997), *Space Dynamics and Control, A Practical Engineering Approach*, Cambridge University Press.

Song, G. & Agrawal, B. N. (2001), 'Vibration suppression of flexible spacecraft during attitude control', *Acta Astronautica* **Vol. 49**.

Topland, M. P. (2004), Nonlinear attitude control of the micro-satellite eseo, Master's thesis, NTNU, Department of Engineeering Cybernetics.

Wertz, J. R. & Larson, W. J. (1999), *Space Mission Analysis and Design*, Microcosm Press and Kluwer Academic Publishers.

Wie, B. (1998), *Space Vehicle Dynamics and Control*, American Institute of Aeronautics and Astronautics, Inc.

Yan, Q., Kapila, V. & Sparks, A. G., eds (2000), *Pulse-Based Periodic Control for Spacecraft Formation Flying*, Proceedings of the American Control Conference, Chicago, Illinois.

Yan, Q., Yang, G., Kapila, V. & de Queiroz, M. S., eds (2000), *Nonlinear Dynamics and Output Feedback Control of Multiple Spacecraft in Elliptical Orbits*, Proceedings of the American Control Conference, Chicago, Illinois.

Yang, G., Yang, Q., Kapila, V., Palmer, D. & Vaidyanathan, R. (2002), 'Fuel optimal maneuvers for multiple spacecraft formation reconfiguration using multi-agent optimization', *International Journal of Robust and Nonlinear Control* **Vol. 12**.

Ye, H., Michel, A. N. & Hou, L. (1998), 'Stability theory for hybrid dynamical systems', *IEEE Transactions on Automatic Control* **Vol. 43, No. 4**.

Yeh, H.-H., Nelson, E. & Sparks, A., eds (2000), *Nonlinear Tracking Control for Satellite Formations*, Proceedings of the 39th IEEE Conference on Decision and Control, Sydney, Australia.

Yeh, H.-H. & Sparks, A., eds (2000), *Geometry and Control of Satellite Formations*, Proceedings of the American Control Conference, Chicago, Illinois.